

Wind Stress Forcing of the Ocean in the SOC Climatology: Comparisons with the NCEP–NCAR, ECMWF, UWM/COADS, and Hellerman and Rosenstein Datasets

SIMON A. JOSEY, ELIZABETH C. KENT, AND PETER K TAYLOR

James Rennell Division, Southampton Oceanography Centre, Southampton, United Kingdom

(Manuscript received 30 August 2000, in final form 26 October 2001)

ABSTRACT

Results from an analysis of the Southampton Oceanography Centre (SOC) global wind stress climatology, which is based on in situ reports for the period 1980–93, are presented. The accuracy of the SOC stresses has been assessed at several locations by comparison of individual monthly means with measurements from Woods Hole Oceanographic Institution research buoy deployments. For the subduction buoy array, situated in the subtropical North Atlantic, the random error in the SOC individual monthly mean wind stress ranges from 0.004 to 0.008 N m⁻², which corresponds to between 5% and 10% of the mean stress depending on which buoy is considered. The large-scale characteristics of the SOC fields are compared with those of the NCEP–NCAR and ECMWF atmospheric model reanalyses, and the in situ observation based on the University of Wisconsin–Milwaukee/Comprehensive Ocean–Atmosphere Dataset (UWM/COADS) and Hellerman and Rosenstein (HR) climatologies. The NCEP–NCAR fields show noticeably weaker wind stress forcing in the Tropics than SOC, while ECMWF and UWM/COADS are in good agreement. From the Tropics to the midlatitudes, the HR stresses tend to be stronger than SOC and the other recent climatologies. At higher latitudes, differences in the spatial structure of the Northern Hemisphere subpolar gyres in SOC and HR are found that are consistent with variations in the state of the North Atlantic and North Pacific Oscillations within the periods on which the climatologies are based. A detailed comparison of the wind-driven response of the ocean is presented for SOC and HR. The North Atlantic subpolar gyre is more intense in SOC than HR and this leads to a doubling in the strength of the Ekman suction. January mean upwelling velocities in this region deduced from the two datasets are 18.9 and 8.6 m month⁻¹, respectively. In the North Pacific a single large-scale subpolar gyre is evident in SOC compared with two smaller gyres in HR. Seasonal to interannual variability in the wind-driven ocean response is quantified using an extended version of the SOC dataset covering the period 1980–97. Significant variability in the Ekman transport across several latitudes that correspond to WOCE hydrographic sections is observed and related to the major atmospheric pressure oscillations.

1. Introduction

The circulation of the upper ocean is driven to a large extent by the transfer of momentum from the atmosphere across the air–sea interface (e.g., Gill 1982). Climatological fields of the momentum transfer, or equivalently the wind stress forcing, have historically been determined from ship meteorological reports. In such analyses, individual estimates of the momentum transfer are determined from the following formula that relates the wind stress τ to the square of the wind speed u ,

$$\tau = \rho C_D u^2, \quad (1)$$

where C_D is the drag coefficient, which incorporates the dependence of the transfer on atmospheric stability, and ρ the air density.

In this paper, we present an evaluation of a global

wind stress climatology produced at the Southampton Oceanography Centre (SOC) from in situ reports covering the period 1980–93. The accuracy of the fields is assessed locally using available measurements from various Woods Hole Oceanographic Institute (WHOI) research buoys. Their large-scale characteristics are compared with those from the recent atmospheric model reanalyses at the National Center for Environmental Prediction–National Center for Atmospheric Research (NCEP–NCAR) and the European Centre for Medium-Range Weather Forecasts (ECMWF), and the earlier in situ based analyses of Hellerman and Rosenstein (1983, referred to as HR hereafter) and da Silva et al. [1994, referred to as UWM/COADS (University of Wisconsin–Milwaukee/Comprehensive Ocean–Atmosphere Dataset)]. In addition to these comparisons, we investigate in detail the consequences of differences in the SOC and HR fields for the wind driven response of the ocean with the focus being on the Northern Hemisphere basins. We have in part been motivated by the observation that despite the recognized deficiencies with the

Corresponding author address: Simon Josey, Room 254/31, James Rennell Division, Southampton Oceanography Centre, European Way, Southampton SO14 3ZH, United Kingdom.
E-mail: Simon.A.Josey@soc.soton.ac.uk

HR climatology, arising from the choice of an unrealistically strong drag coefficient (Harrison 1989), its use in both hydrographic and modeling studies remains widespread (e.g., Smith et al. 2000). In addition, we wish to establish the principal characteristics of the SOC fields as they are now finding application in both modeling and hydrographic studies (e.g., Megann and New 2001; Bryden and Beal 2001).

The SOC fields have been determined from a dataset of meteorological reports that has, for the first time, been corrected at the level of individual ships for various biases arising from observing procedure (Kent et al. 1993a,b; Kent and Taylor 1997). The wind stress estimates have been determined using the drag coefficient relationship of Smith (1980), which is in good agreement with the results of a recent analysis of wind stress measurements made on research ships in which the effects of airflow distortion by the ship structure have been taken into account (Yelland et al. 1998). The SOC wind stress fields are thus expected to be the most accurate currently available from ship observations.

In addition to its dependence on atmospheric stability, the drag coefficient varies with wind speed. A large amount of research has been devoted to quantifying this relationship (e.g., Smith 1980; Large and Pond 1981; Yelland et al. 1998) and to establishing whether it is also dependent on parameters describing the sea state, in particular the wave age and steepness (e.g., Bonekamp et al. 2002; Taylor and Yelland 2001). Values for the drag coefficient employed in early climatological analyses (Bunker 1976; HR) are now thought to have been significantly overestimated. In particular, the scheme employed by HR leads to a drag coefficient typically about 25% greater than that generally accepted today (WGASF 2000). As the wind driven response of the ocean, via the Ekman transport and upwelling rates, scales directly with the magnitude of the wind stress, the consequences of an overestimate of this magnitude for the many studies that have made use of the HR fields are potentially significant. Such studies include the use of climatological estimates of the Ekman transport in combination with hydrographic section measurements for determining ocean heat and freshwater transports, and the use of the wind fields for forcing ocean models.

Several other analyses of the wind forcing of the ocean based on ship meteorological reports have been carried out subsequent to HR and these are summarized briefly here. Harrison (1989), referred to as Harrison hereafter, noted the bias in the HR fields arising from the choice of drag coefficient. He produced an alternative climatology using a similar ship dataset to that employed by HR and the more accurate drag coefficient scheme of Large and Pond (1981), which gave rise to smaller values than that adopted by HR. Consequently the stress estimates obtained by Harrison were reduced in magnitude by approximately 20% relative to HR. We note that various ocean model studies have subsequently provided additional evidence that the HR stresses are

overestimates (e.g., Gordon and Corry 1991). Surprisingly, the Harrison climatology has not found widespread use among the oceanographic community. Isemer and Hasse (1987) produced a revised analysis of the Bunker (1976) North Atlantic wind stress fields. They used a drag coefficient scheme that gave rise to values similar in magnitude to those of Large and Pond (1981), that is, weaker than those originally employed by Bunker (1976). However, the resulting stresses were similar in strength to Bunker's original fields as the reduction in the drag coefficient was compensated to a large extent by an increase in the mean strength of visually estimated winds resulting from the use of the revised Beaufort scale of Kaufeld (1981). Lindau (1995) and Kent and Taylor (1997) have subsequently shown that the Kaufeld (1981) scale leads to visual winds that are biased high in the mean when compared to anemometer-based estimates. Thus, the Isemer and Hasse (1987) stresses are expected to overestimate the true values in the North Atlantic. Da Silva et al. (1994) produced the UWM/COADS global wind stress climatology using ship reports for the period 1945–89, their own visual wind scale and a version of the Large and Pond (1981) scheme modified at low wind speeds. Finally, Gulev and Hasse (1998) have developed a wind stress climatology for the North Atlantic using a wave-age-dependent drag coefficient. They find that the inclusion of a wave age dependence leads to an enhancement of the monthly mean wind stress in winter by 10%–20% at mid-high latitudes. However, Taylor and Yelland (2001) find no evidence for such a dependence in their recent analysis of observational data and suggest instead that the sea surface roughness is determined solely by the significant wave height and peak wavelength of the combined sea and swell spectrum.

The analyses of HR and Harrison are based on data collected over long periods (1870–1976 for HR; 1850–1979 in the Atlantic/Indian Ocean and 1950–79 in the Pacific Ocean for Harrison) in which there were significant fluctuations in the quality and spatial distribution of the meteorological reports and hence the wind stress estimates. In the SOC analysis, data from a more recent period were employed. Consequently, the SOC stress fields reflect the state of the wind forcing of the oceans at the time of the World Ocean Circulation Experiment (WOCE), within which a large number of hydrographic sections were undertaken. We expect the SOC fields to exhibit significant regional differences from the HR climatology as a result of the influence of the major atmospheric pressure oscillations. In particular, the North Atlantic Oscillation is known to have been in a predominantly positive state; that is, the Azores High/Iceland Low pressure contrast has been particularly strong since the early 1980s (Hurrell 1995; Dickson et al. 1996). Thus we expect stronger features associated with the North Atlantic subpolar gyre in the SOC analysis.

Atmospheric model reanalyses that assimilate in situ

data and in some cases satellite observations of the surface wind speed [for details of data types assimilated see WGASF (2000)] have provided increasingly important alternative sources of stress estimates in recent years (e.g., Kalnay et al. 1996; Kallberg 1997). Each potentially avoids the sampling problems that beset ship-based analyses although assimilation of satellite data does not necessarily lead to more accurate fields. Trenberth et al. (1990) prepared a wind stress climatology from ECMWF operational model output for the period 1980–86 and noted significantly stronger zonal stresses than HR in the Southern Ocean, a region virtually unsampled by ships. However, the accuracy of such fields remains dependent to a large extent on the model physics. The same authors noted that the ECMWF model was unable to adequately reproduce the convergent characteristics of the wind stress fields in the tropical Pacific. Further, an intercomparison of operational model output from the ECMWF and the former National Meteorological Center lead Trenberth and Olson (1988) to conclude that differences between the models were likely to lead to errors of 15%–25% in surface wind stress at midlatitudes. We will show that significant differences remain between the modern counterparts of these fields from the ECMWF and NCEP–NCAR reanalyses. The satellite datasets are restricted to a relatively short time period and for reasons of brevity we have not considered them in detail in the present analysis, although we believe they will become increasingly important in the future.

In contrast to the flux of heat across the air-sea interface, evaluation of the wind stress fields is hampered by the lack of large-scale constraints. The surface heat exchange can be globally constrained by the requirement that the mean net heat flux average to zero and regionally constrained using hydrographic estimates of the ocean heat transport (e.g., Josey et al. 1999). However, it is difficult to use integral measures of the ocean response for assessing biases in the wind stress fields. Determinations of the integrated Sverdrup transport from climatological stresses have been compared in the North Atlantic with measurements of the return flow through the Straits of Florida (Leetmaa and Bunker 1978; Böning et al. 1991). However, there has been considerable debate over whether the Sverdrup balance provides a meaningful statistic for this comparison (Wunsch and Roemmich 1985). Comparisons with the measured seasonal variation in the Florida straits transport have been forced to rely on wind-driven ocean models (Fanning et al. 1994), as the effects of bottom topography have to be considered, and uncertainties over model physics have limited the usefulness of this approach for assessment of biases in the forcing stresses. Given the above limitations, we have focused on local rather than large-scale constraints in the evaluation of the SOC wind stresses in the present study.

In the following section, we describe the data source, outline the method used to produce the climatological

fields, and present results from the comparison of the SOC stresses with research buoy measurements. In section 3, we compare the SOC global wind stress fields with NCEP–NCAR, ECMWF, UWM/COADS, and HR. In addition we assess the impact of the differences between SOC and HR on the wind driven response of the ocean in the North Atlantic and North Pacific. We note that our focus is on the mid-high latitudes and we do not discuss in detail the characteristics of the wind stress fields in the Tropics. Finally, we summarize our findings and draw some conclusions with regard to the choice of a representative wind stress field for use in hydrographic and modeling studies.

2. Wind stress estimation and evaluation

A detailed description of the surface meteorological report dataset and method used to generate the SOC climatology is given in Josey et al. (1998). Here we provide only a brief description of the points relevant to the wind stress fields and highlight the main differences with respect to the other climatologies considered.

a. The surface meteorological report datasets

The SOC wind stress estimates have been obtained from a modified version of the Comprehensive Ocean–Atmosphere Dataset release 1a (Woodruff et al. 1993) onto which additional metadata describing observing procedure has been merged from the International List of Selected, Supplementary and Auxiliary Ships (WMO47: WMO 1993). The merged dataset contains approximately 30 million in situ meteorological reports covering the period 1980–93. Using the additional metadata the reports have been individually corrected for the first time for various observational biases identified in an analysis of Voluntary Observing Ship (VOS) observations (Kent et al. 1993a,b). Hellerman and Rosenstein used an earlier uncorrected in situ dataset that spanned the significantly longer period, 1870–1976, but contained a similar number of reports (due primarily to the much smaller contribution from buoys). For UWM/COADS, da Silva et al. (1994) used the earlier COADS Release 1 (Woodruff et al. 1987), which spanned the period 1945–89. The NCEP–NCAR and ECMWF reanalyses assimilate a variety of observations including surface meteorological reports of the type included in COADS (for details see Kalnay et al. 1996; Kallberg 1997).

b. Method of calculation

Estimates of the zonal, τ_x , and meridional, τ_y , components of the sea surface wind stress for each in situ report have been obtained using (1) expressed in component form

$$\begin{aligned}\tau_x &= \rho C_D u_x (u_x^2 + u_y^2)^{1/2} \\ \tau_y &= \rho C_D u_y (u_x^2 + u_y^2)^{1/2},\end{aligned}\quad (2)$$

where u_x and u_y are the zonal and meridional components of the wind speed, respectively. The drag coefficient values used in the above equation depend upon the height of the wind measurement and the atmospheric stability. The wind data reported by the VOS are estimated either visually or from an anemometer readout. Visual wind estimates were corrected to the Beaufort equivalent scale of Lindau (1995), which had been found to give the best correspondence between monthly mean $1^\circ \times 1^\circ$ wind speeds from anemometers at known heights and corresponding visual means for a subset of the merged data (Kent and Taylor 1997). The reported wind speeds were converted to 10-m neutral stability values u_{10n} using an iterative procedure with the flux-profile relationships and transfer coefficients defined by Smith (1988, 1989) except that we have adopted the 10-m neutral drag coefficient C_{D10n} relationship of Smith (1980)

$$10^3 C_{D10n} = 0.61 + 0.063u_{10n}. \quad (3)$$

For measured winds the anemometer height for each individual ship was obtained from the merged metadata from WMO47. Default anemometer heights were applied where no information was available as follows: ships (20 m), buoys (8 m), and platforms (80 m). Visual winds were assumed to be equivalent to measurements at 25 m (Lindau 1995) under neutral conditions. Since ship anemometers are typically mounted at between 15 and 40 m, the height correction to 10 m reduces measured and visual wind speed values, whereas for winds up to and including Beaufort force 8 (i.e., $\leq 19 \text{ m s}^{-1}$), the adjustment to the Lindau (1995) scale increases the visual wind values. The overall effect of the adjustments was to decrease the wind speed data obtained in higher latitudes by about $0.5\text{--}1 \text{ m s}^{-1}$ in the Atlantic. In the Pacific the proportion of anemometer-derived winds was greater and the instruments were mounted higher (Taylor et al. 1999), resulting in a typical decrease of $1.0\text{--}1.5 \text{ m s}^{-1}$. In the lighter winds of tropical and subtropical regions the typical adjustments were less than 0.5 m s^{-1} and of either sign.

Hellerman and Rosenstein adopted a quadratic form for the drag coefficient dependence on wind speed and stability (expressed as the air-sea temperature difference), obtained from a least squares fit to values tabulated in an earlier study of the North Atlantic climate by Bunker (1976). Bunker's values were based on a survey of previous studies, mostly review papers, of the $C_{D10n}-u_{10n}$ relationship. The original data quoted in these studies were predominantly obtained over lakes or sheltered sea locations (such as the Baltic or North Sea) where observed drag coefficients tend to be significantly larger than for the open ocean [e.g., see the review of Geernaert (1990)]. Under neutral conditions the HR relationship takes the form:

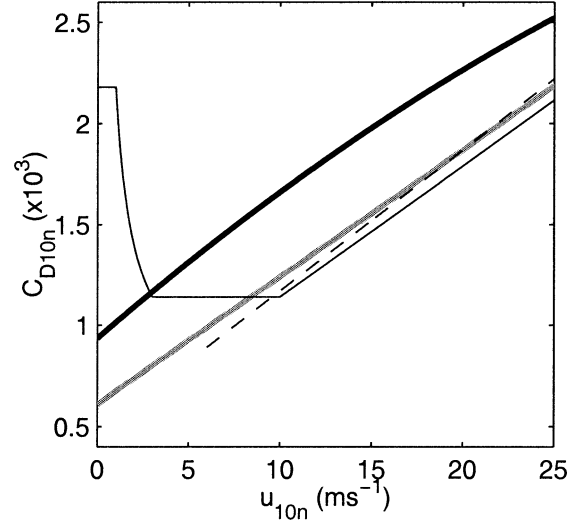


FIG. 1. Variation of the neutral drag coefficient C_{D10n} (multiplied by 10^3) with the 10-m neutral wind speed u_{10n} . Solid gray line: Smith (1980); dashed black line: Taylor and Yelland (2000); solid thick black line: HR; solid thin black line: UWM/COADS.

$$10^3 C_{D10n} = 0.934 + 0.0788u - 0.000616u^2, \quad (4)$$

which results in values for C_{D10n} that are 28% greater on average than obtained with Smith (1980) in the wind speed range $5\text{--}25 \text{ m s}^{-1}$ (see Fig. 1). Bunker (1976) stated that the wind speed value [u in Eq. (4)] should be obtained at 10-m height, or at the height of measurement, but did not apply any height corrections. This was reasonable since the fraction of anemometer measurements was negligible before 1960 (Taylor et al. 1995) and the visual wind scale in use ("WMO1100") defined a 10-m wind value. Similarly it would appear that HR used the visual wind estimates as reported and did not adjust measured winds for the effect of the anemometer height.

To summarize, the individual wind stress values calculated by ourselves compared to those of HR might differ due to the different observation types and calculation methods used. The wind values in the HR dataset were predominantly visual estimates. Since 1970 the fraction of anemometer winds has increased rapidly, reaching 80% in the Pacific and 40% in the North Atlantic by the mid 1980s (Taylor et al. 1999). For the time period discussed in this paper the observations are a mix of visual and anemometer values in the Atlantic and predominantly anemometer values elsewhere. By adjusting visual winds to the Lindau (1995) scale we have ensured that they are compatible with the anemometer winds and we have taken account of the height of the anemometers by adjusting all winds to 10 m. Fortunately the difference between the Lindau (1995) and WMO1100 scales on average is small, suggesting that the differences due to these significant changes in observation technique may also be small. Thus the most significant difference is expected to be due to the dif-

ferent C_{D10n} - u_{10n} relationships chosen. As noted in the introduction, the choice of Smith (1980) for the drag coefficient was based on the open ocean measurements of Yelland et al. (1998). Later reanalysis of these data has served to confirm that choice (Taylor and Yelland 2000). In contrast the C_{D10n} - u_{10n} relationship used by HR was based on data that were predominantly from lakes and enclosed seas and would be expected to overestimate the open ocean wind stress.

For UWM/COADS, da Silva et al. (1994) developed their own correction to visual wind estimates for biases in the WMO1100 scale. Kent and Taylor (1997) found that the da Silva et al. (1994) correction leads to similar results to those obtained with the Beaufort equivalent scale of Lindau (1995) employed for the SOC analysis. The C_{D10n} - u_{10n} relationship adopted for UWM/COADS, shown in Fig. 1, is based on Large and Pond (1981) with a modification at low wind speeds that leads to stronger stresses. Wind stress estimates in the NCEP-NCAR and ECMWF reanalyses are also obtained using the bulk formula (2) approach: the C_{D10n} schemes employed have been well reviewed recently by Renfrew et al. (2002) and we refer the reader to that paper for full details.

In the SOC analysis, outliers (i.e., unrealistically high or low wind stress estimates resulting, e.g., from observational error or misreporting of the ship's position) were removed from the dataset of individual wind stress estimates prior to averaging to form climatological mean fields. A given stress estimate was removed if any of the surface meteorological variables on which it depended lay outside the climatological 4.5σ limits that are defined within COADS1a [see Woodruff et al. (1993) for definition of σ]. Raw mean wind stress fields were generated from the resulting trimmed dataset by averaging over individual reports for each month in the period January 1980–December 1993 on a $1^\circ \times 1^\circ$ grid from 85°S – 85°N . The raw fields were then smoothed and estimates obtained in the unsampled regions of the grid using a simple successive correction method in which an analyzed mean is produced from the raw mean estimates within a certain radius of influence, the value of which is reduced from a maximum of 1541 km to a minimum of 331 km during the analysis [see Josey et al. (1998) for full details and Kent et al. (2000) with regard to the resulting resolution]. Finally, climatological monthly mean fields were generated from the individual monthly analyzed fields for 1980–93. Note that the flux dataset has subsequently been extended to 1997 using an extension to the COADS1a (S. Worley and S. Woodruff 1999, personal communication) for which wind stress fields were calculated using the same method described above including the corrections for observational bias. Results obtained with the extended dataset are also presented in several sections.

The procedure adopted for the SOC analysis was based on that originally used for UWM/COADS. The main differences are that da Silva et al. (1994) used 3.5σ

σ limits for removing outliers (note that 4.5σ limits were not available with COADS1) and a larger minimum radius of influence, 771 km. The same $1^\circ \times 1^\circ$ grid was employed in both cases. Regarding the reanalyses, we have used a subset of the first version (Reanalysis 1: Kalnay et al. 1996) of the NCEP-NCAR fields for the period 1979–1998, interpolated from the original Gaussian grid onto a global $2.5^\circ \times 2.5^\circ$ grid (supplied by G. White, NCEP). For ECMWF we have considered the fields from the full reanalysis (Kallberg 1997), which covers the period 1979–93, interpolated onto a global $1.125^\circ \times 1.125^\circ$ grid (supplied by B. Barnier, LEGI-IMG).

In HR, the analysis was carried out on a $2^\circ \times 2^\circ$ grid and outliers were not removed prior to averaging. The climatological monthly fields were produced by averaging over all reports in a given box and month within the full period (1870–1976) rather than by first forming individual monthly means and then averaging over those to produce climatological values. The resulting fields were smoothed using a Laplacian operator, which included a dependence on the number of observations; see HR for details. The HR grid runs from 84°S to 84°N and for several of the comparisons presented here the SOC fields have been averaged onto the same grid. It is important to remember that in both climatologies the distribution of ship reports, and hence of estimated stresses, shows strong spatial variations (e.g., Fig. 2 of Josey et al. 1998). In particular, large areas with very few observations occur in the Southern Ocean and southeast Pacific and care must be exercised in attaching significance to the fields in these regions.

Hellerman and Rosenstein took the standard error of the mean as a measure of confidence in their fields (see their Fig. 5). However, such an approach is potentially misleading as it provides a measure of the random error due to observational error and sampling limitations but gives no information on possible systematic errors in the fields. Estimation of the random errors in ship-based climatological flux fields is a complex task (Gleckler and Weare 1997). A comprehensive analysis of the errors for the wind stress would require knowledge of the errors in the original meteorological observations, of the strength of the spatial and temporal correlations between the variables in the wind stress formula, and of the propagation of errors during the objective analysis. Following the method of Lindau (1995), Kent et al. (1999) have determined the random errors in the meteorological observations used in calculating the SOC climatology. However, as discussed in the context of the analysis of the SOC heat fluxes by Josey et al. (1999), at present we do not consider our knowledge of the correlation terms sufficient to use their results to derive error fields. Thus, in the present study our main assessment of the overall accuracy of the calculated stresses is by comparison with measurements from research buoy deployments, which we discuss in the following section.

TABLE 1. Summary of wind stress statistics averaged over the period of each subduction buoy deployment for which reliable observations were available according to Moyer and Weller (1997). Tabulated values are the deployment averages of the monthly mean zonal and meridional components τ_x and τ_y , the wind stress magnitude $|\tau|$, and difference in wind stress magnitude $|\tau|_{SOC} - |\tau|_{Buoy}$, all with units $N\ m^{-2}$, and difference in wind stress direction $\theta_{SOC} - \theta_{Buoy}$, units degrees. Standard errors of the differences and the number of months N_m in each comparison are also listed.

Location	Source	τ_x	τ_y	$ \tau $	$ \tau _{SOC} - \tau _{Buoy}$	$\theta_{SOC} - \theta_{Buoy}$
NE buoy, $N_m = 25$ (33°N, 22°W)	SOC	-0.017	-0.029	0.048	0.007 ± 0.004	9.5 ± 6.4
	Buoy	-0.016	-0.027	0.041		
SE buoy, $N_m = 15$ (18°N, 22°W)	SOC	-0.050	-0.084	0.099	-0.009 ± 0.005	3.4 ± 1.0
	Buoy	-0.050	-0.094	0.108		
SW buoy, $N_m = 16$ (18°N, 34°W)	SOC	-0.090	-0.036	0.098	0.013 ± 0.008	0.9 ± 2.4
	Buoy	-0.077	-0.032	0.085		
NW buoy, $N_m = 13$ (33°N, 34°W)	SOC	-0.011	0.000	0.039	0.010 ± 0.004	13.7 ± 7.0
	Buoy	-0.015	0.000	0.029		
C buoy, $N_m = 20$ (25.5°N, 29°W)	SOC	-0.048	-0.021	0.059	0.000 ± 0.006	10.1 ± 4.1
	Buoy	-0.049	-0.027	0.059		

c. Evaluation of the SOC stresses against research buoy measurements

In this section, the accuracy of the individual monthly mean estimates used to generate the SOC climatological wind stress fields is evaluated at several locations by comparison with estimates based on high-frequency wind speed measurements from various WHOI meteorological buoy deployments. A similar evaluation has been carried out for the SOC heat flux estimates, and a more detailed description of the deployments used for the comparison and the limitations of this technique can be found in Josey et al. (1999) and Josey (2001).

1) COMPARISON METHOD

Measurements from WHOI buoys deployed in several different ocean regions for periods ranging from four months to two years (Weller and Anderson 1996; Weller et al. 1995; Moyer and Weller 1997; Weller et al. 1998) have been used for the comparison (see Tables 1 and 2). For details of the buoy instrumentation see Moyer and Weller (1997); estimates of the monthly average wind stress were determined from 1-min mean wind speed measurements using the Coupled Ocean–Atmosphere Response Experiment (COARE) algorithm (Fairall et al. 1996). The WHOI group have estimated the typical accuracy of the buoy-measured monthly mean stresses to be in the range $0.001\text{--}0.002\ N\ m^{-2}$. The buoy stresses have the advantage of being determined from relatively high-frequency wind speed measurements made under all weather conditions. By comparing them against the

SOC stresses we are therefore able to determine whether the SOC estimates are biased as a result of the relatively low frequency of the in situ observations on which they are based and by the possible avoidance by ships of severe weather conditions. For our analysis, monthly mean stresses from the WHOI buoys were compared with collocated values from the SOC wind stress dataset for the buoy deployment period (the term “dataset” refers to the monthly means from individual years as opposed to “climatology,” which refers to the monthly means averaged over the period 1980–93). Note that data from these buoys were not included in the merged COADS1a/WMO47 dataset, and that measurements from the Arabian Sea buoy were compared with fields extracted from the extension to the SOC flux dataset (see section 2a). Note also that we have not used observations from the Tropical Atmosphere–Ocean array (McPhaden et al. 1998) in our comparison as these were included in the merged dataset used to produce the SOC fields and so cannot be regarded as an independent dataset for validation purposes.

2) COMPARISON RESULTS

Time series of the wind stresses from the buoys and the SOC dataset, expressed as vectors for each month, are shown in Figs. 2 and 3. Summary statistics are listed in Tables 1 and 2. The tabulated values are deployment averages of the monthly mean values of the components τ_x and τ_y and the monthly mean wind stress magnitude, $|\tau|$. Also listed are the mean difference in wind stress

TABLE 2. As in Table 1 but for the Arabian Sea, TOGA, and FASINEX buoy deployments.

Location	Source	τ_x	τ_y	$ \tau $	$ \tau _{SOC} - \tau _{Buoy}$	$\theta_{SOC} - \theta_{Buoy}$
Arabian Sea, $N_m = 13$ (15.5°N, 61.5°E)	SOC	0.058	0.039	0.106	0.015 ± 0.012	-7.2 ± 6.6
	Buoy	0.036	0.020	0.091		
TOGA, $N_m = 4$ (1.75°S, 156°E)	SOC	0.021	-0.009	0.026	0.000 ± 0.004	-10.6 ± 1.5
	Buoy	0.020	-0.012	0.026		
FASINEX, $N_m = 4$ (27°N, 70°W)	SOC	0.015	0.000	0.031	0.007 ± 0.003	16.5 ± 27.2
	Buoy	0.006	0.000	0.024		

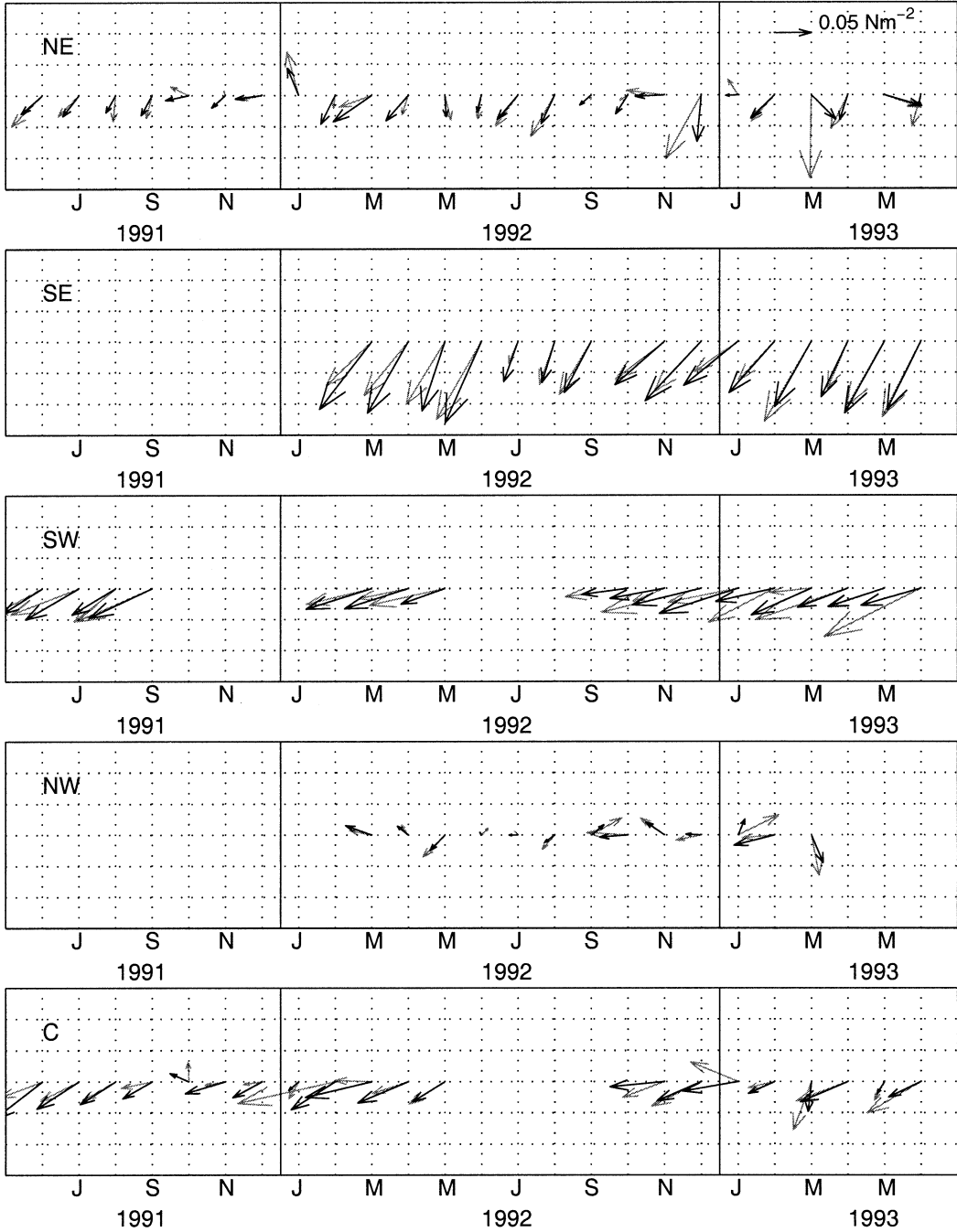


FIG. 2. Time series of buoy (black arrows) and SOC (gray) wind stress estimates at the various subduction buoy sites for those months for which reliable buoy data were available. All panels are shown to the same scale.

magnitude and direction between SOC and each buoy; note that a positive value for directional difference implies that the SOC estimate differs in a clockwise sense from the buoy.

(i) The subduction buoy array

The Subduction Experiment buoys were deployed in the eastern North Atlantic between 18° and 33°N . The

buoy and SOC wind stresses are generally in good agreement, with much of the intermonth variability being captured by the SOC dataset (see Fig. 2). At four of the five sites, the SOC and buoy estimates for the scalar mean wind stress agree to within a two standard error limit. At the remaining site, the NW buoy, the SOC stresses lie slightly outside this limit although the difference remained relatively small, 0.010 N m^{-2} in the mean. Good directional agreement was also found

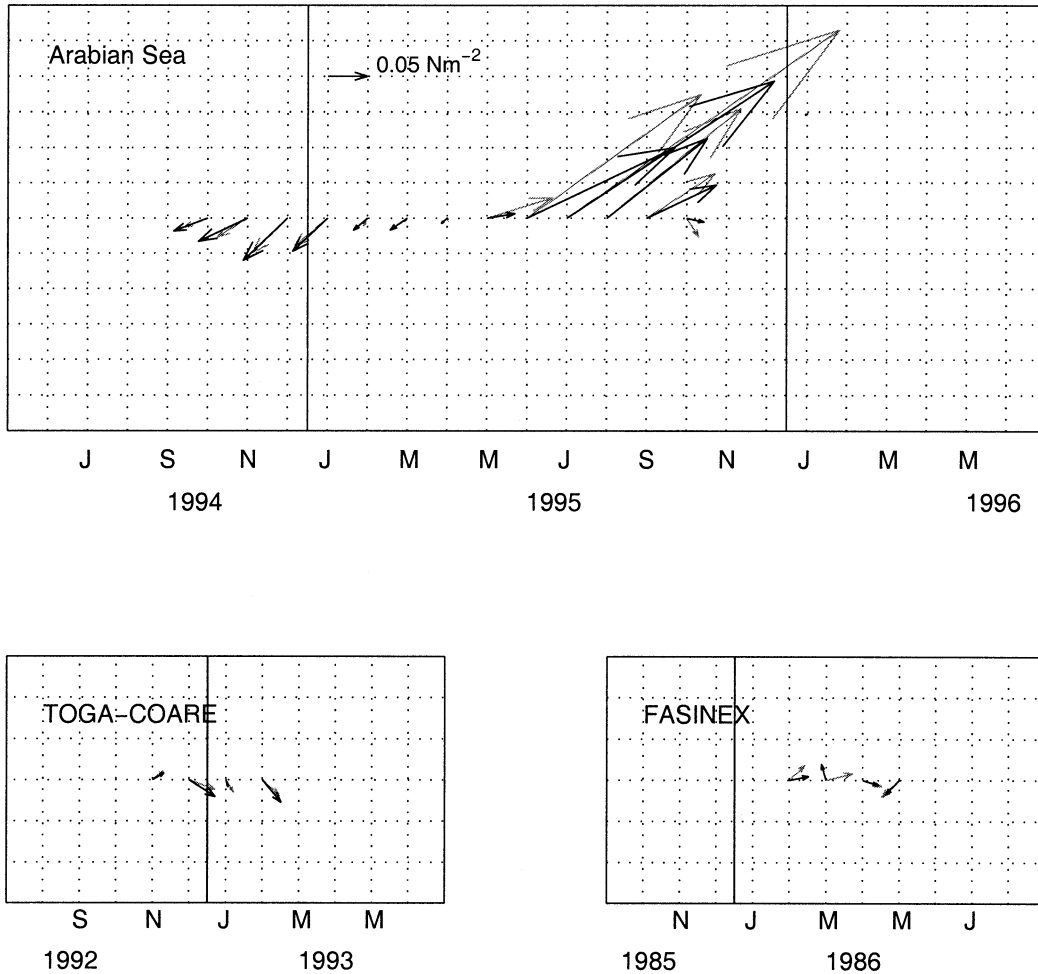


FIG. 3. Time series of buoy (black arrows) and SOC (gray) wind stress estimates at the Arabian Sea, TOGA COARE, and FASINEX buoys. All panels are shown to the same scale.

between the SOC and buoy stresses, the mean difference ranged from 0.9° to 13.7° .

(ii) The Arabian Sea buoy

At the Arabian Sea site, the strong monsoon related variations in wind direction measured by the buoy were in good agreement with SOC (see Fig. 3). However, during the southwest monsoon months of June–August, the SOC mean scalar stress, 0.313 N m^{-2} , was approximately 30% greater than the buoy value, 0.234 N m^{-2} . Possible sources for this difference include sensor error and variations in the behavior of the stress algorithms at high wind speeds. The COARE algorithm has lower values for the drag coefficient than Smith (1980) under strong wind speed conditions (WGASF 2000). The possibility that this variation is the source of the difference has been explored by calculating the pseudostress magnitude (i.e., wind speed squared), which is independent of the chosen bulk parameterization. The results show similar behavior to the full stress estimates, with the SOC value for the pseudostress magnitude for June–

August, $161.3 \text{ m}^2 \text{ s}^{-2}$, being 20% greater than that for the buoy, $134.6 \text{ m}^2 \text{ s}^{-2}$. Thus, variations between the algorithms may at most be responsible for only a relatively small proportion of the observed difference. Time series of the wind speed for each dataset (not shown) reveal that the buoy-measured wind speed became biased low relative to the SOC value after April 1995, at which time the sensor used for the first part of the deployment was replaced. Prior to the sensor change the mean difference (buoy–SOC) and standard error of the monthly averaged wind speeds was $0.2 \pm 0.2 \text{ m s}^{-1}$, after the change a significant offset developed that persisted throughout the remainder of the deployment, the difference being $-1.1 \pm 0.1 \text{ m s}^{-1}$. Thus, it appears that the bias found here during the southwest monsoon probably reflects sensor error rather than variations in the algorithms employed.

A further possible source of the bias are gradients of the wind stress within the grid cell containing the buoy, which when coupled with the irregular distribution of ship estimates used to form the SOC wind stress value

have the potential to lead to a bias. A simple estimate of the gradient of wind stress across the $1^\circ \times 1^\circ$ SOC grid cell centered on the buoy location has been determined by interpolation of the SW monsoon SOC wind stress values within a buoy centered $5^\circ \times 5^\circ$ square to provide values at the central cell boundaries. In the extreme case where the SOC estimate is representative of the cell boundary rather than the center as a result of the distribution of ship observations, the intragrid differences of boundary and center values are then approximately 0.02 N m^{-2} and 0.01 N m^{-2} in the east–west and north–south directions, respectively. The difference between the buoy and SOC was found to be 0.08 N m^{-2} , so it is possible that intragrid variations contribute of order 25% of the difference but not that they account for the full bias that was found.

(iii) The TOGA COARE and FASINEX buoys

The Tropical Ocean Global Atmosphere (TOGA)–COARE buoy was deployed in the western equatorial Pacific warm pool from November 1992 to February 1993. During this period the buoy and SOC stress estimates agreed well, both averaged to 0.026 N m^{-2} in the mean and showed a transition from southwesterlies to northwesterlies between November and December 1992. The Frontal Air–Sea Interaction Experiment (FASINEX) moored buoy array consisted of five buoys deployed within 50 km of each other in a region southwest of Bermuda between February and May 1986 (Weller et al. 1995). Array-averaged buoy estimates of the stresses were compared with values from the SOC stress dataset averaged over the box ($26^\circ\text{--}28^\circ\text{N}$, $69^\circ\text{--}71^\circ\text{W}$) centered on the array. Good agreement was found in the last two months of the deployment period, although a significant difference in direction was evident in April 1986.

The above comparisons provide some confidence in the SOC stress estimates at the various buoy locations. An estimate of the random error in the SOC individual monthly means at the subduction buoy sites is provided by the standard error of the wind stress difference (SOC – buoy), which ranges from 0.004 to 0.008 N m^{-2} . This range corresponds to between 5% and 10% of the mean stress depending on which buoy is considered. The climatological monthly means have been formulated from a dataset that spans a 14-yr period. Hence, we expect them to have a random error of order $0.001\text{--}0.002 \text{ N m}^{-2}$ in regions with sampling at a level similar to that for the subduction array [which includes much of the midlatitude Northern Hemisphere basins, see Fig. 2 of Josey et al. (1999)]. The Arabian Sea buoy comparison results were less conclusive: significant differences occurred during the southwest monsoon but these are probably due to an error in the buoy wind speed measurements following a change of sensor. Over the period of the Arabian Sea buoy deployment, the standard error of the mean difference was 0.015 N m^{-2} ;

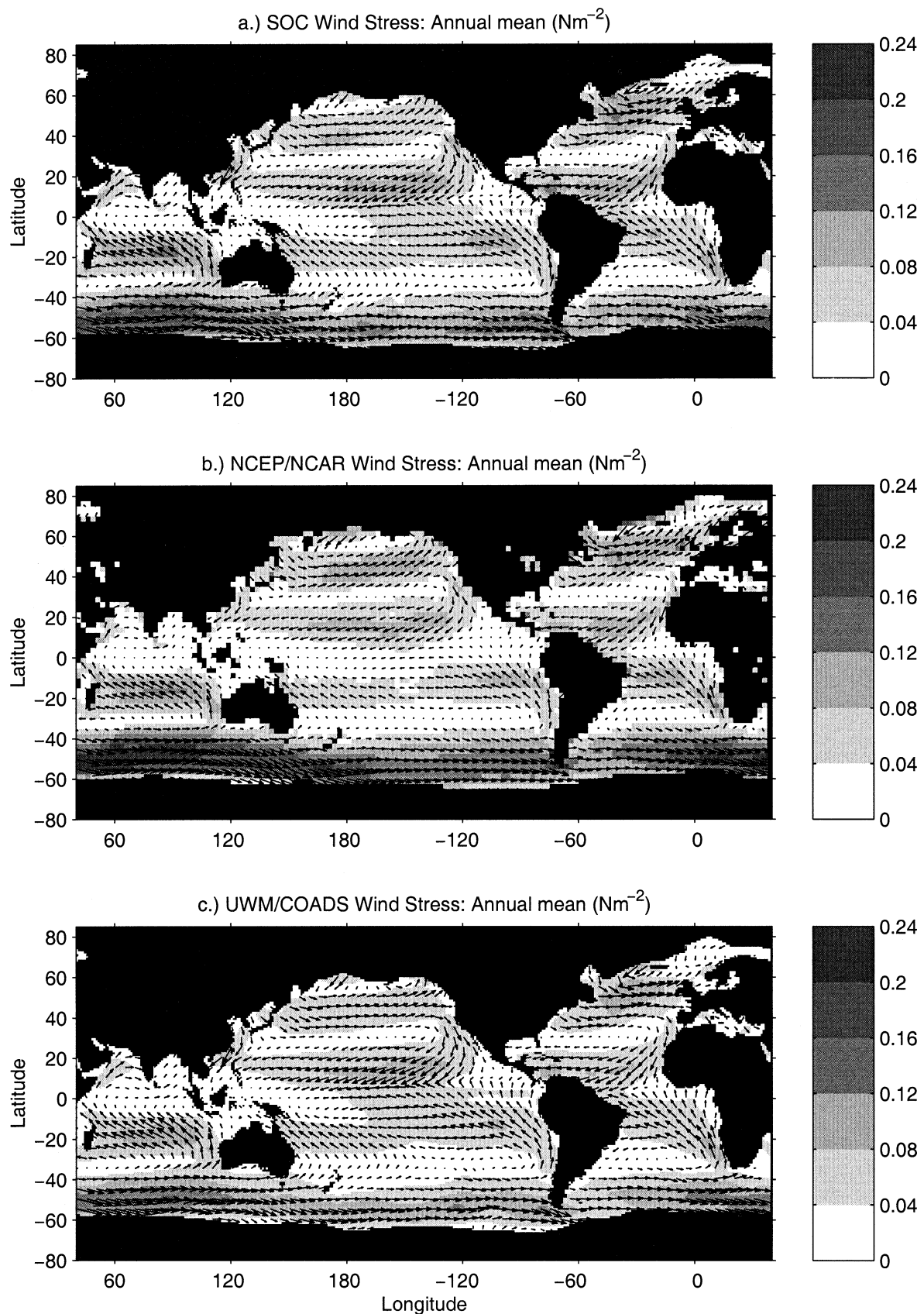
hence we estimate the random error of the climatological monthly mean in this more poorly sampled region to be of order 0.004 N m^{-2} . Although covering a relatively short period, the TOGA buoy comparisons suggest that the SOC monthly stresses are capable of representing subtle directional variations in the relatively weak wind stress forcing of the tropical Pacific warm pool region. Our results demonstrate that the relatively small number of observations from which in situ observation based stress estimates are determined does not lead to them being biased low, as has been suggested in past studies (e.g., Mestas-Nunez et al. 1994) Indeed, inspection of the values in Tables 1 and 2 suggests that the SOC wind stress estimates are slightly higher than the buoy estimates, although this slight positive bias is only significant at the two standard error level for the NW Subduction and FASINEX buoys. We note that use of the HR drag coefficient scheme instead of Smith (1980) would have lead to a significantly increased positive bias with respect to the buoy measurements.

3. Analysis of the wind stress forcing fields

In this section, we compare the SOC global climatological wind stress forcing fields with NCEP–NCAR, ECMWF, UWM/COADS, and HR. The largest differences are found to be between SOC and HR, and we go on to evaluate the impact of these differences on the wind driven response of the ocean with the focus being on the relatively well sampled Northern Hemisphere basins.

a. Climatological mean wind stress

Annual mean maps of the wind stress for each of the climatologies considered are shown in Fig. 4 and the variation of the zonal mean wind stress magnitude with latitude in Fig. 5. The fields are broadly similar in their main features, that is, the subtropical and subpolar gyres, intertropical convergence zone, and the band of intense westerly stresses in the Southern Ocean. However, significant quantitative differences are evident in several cases. In particular, the NCEP–NCAR fields tend to have weaker stresses in the Tropics compared to the other climatologies. The zonal average wind stress magnitude at the Equator for NCEP–NCAR is 0.022 N m^{-2} , compared with 0.031 N m^{-2} for SOC and UWM/COADS, 0.034 N m^{-2} for ECMWF, and 0.041 N m^{-2} for HR. The tropical bias in the NCEP–NCAR stresses is consistent with the results of Smith et al. (1999), who find that the stresses from this reanalysis are systematically low when compared with a sample of high quality estimates obtained from research ships within WOCE. We note that a similar tropical bias was also found by Milliff et al. (1999) from a comparison with scatterometer derived stresses over the relatively short interval August 1996–July 1997 and in an evaluation of pseudostress estimates by Stricherz et al. (1997).



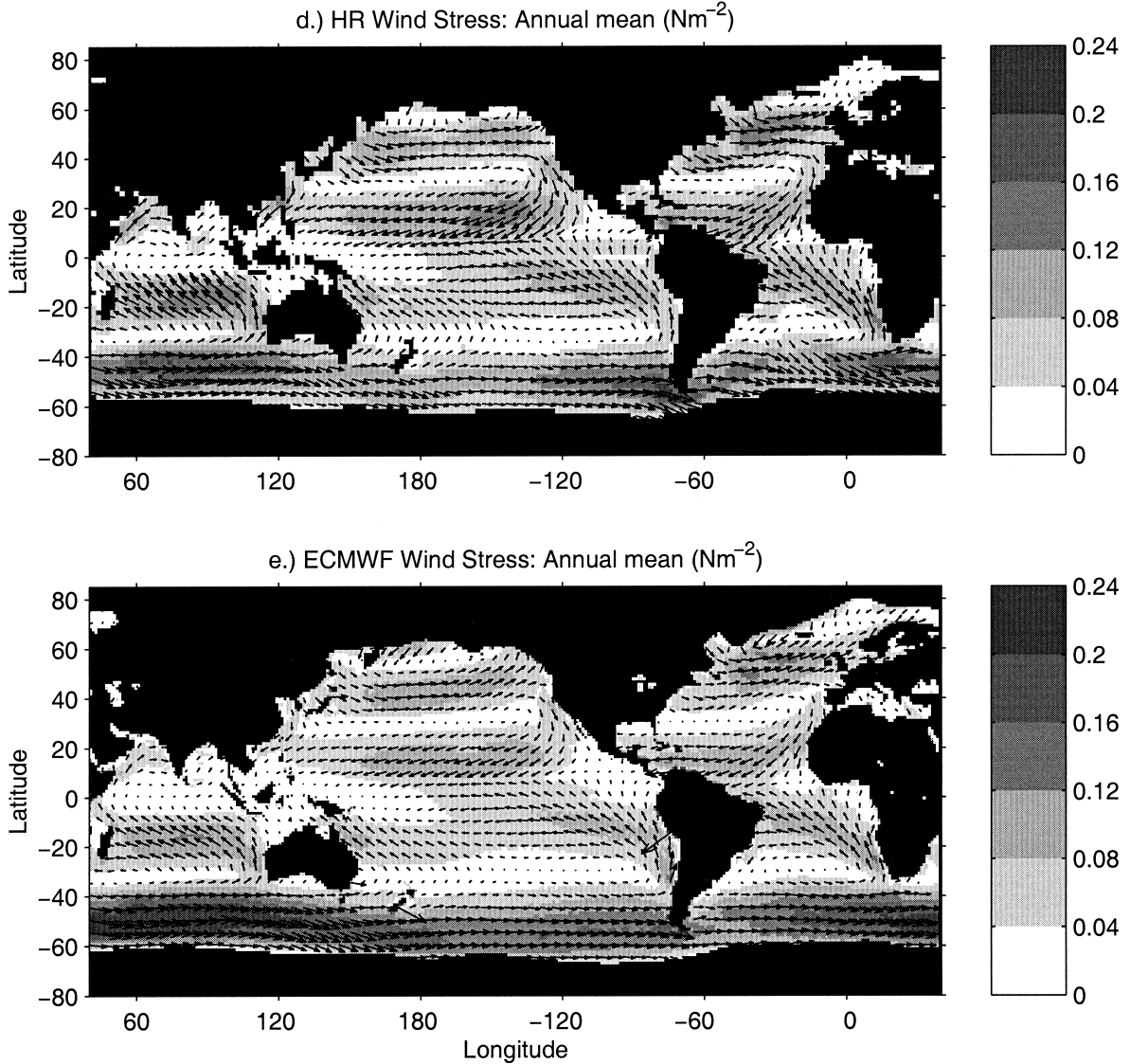


FIG. 4. Climatological annual mean fields for (a) SOC, (b) NCEP–NCAR, (c) UWM/COADS, (d) HR, and (e) ECMWF. Units are N m^{-2} .

The ECMWF fields are in better quantitative agreement with SOC from the Tropics to midlatitudes (see Fig. 5). However, it should be noted that although the ECMWF fields appear reasonable at the basin scales shown here they are known to exhibit strong wavelike variations in several regions at scales of order several hundred kilometers and very high values for the stress at a number of island sites, for example, the South Island of New Zealand. The wavelike variations are a recognized topographically induced problem with the ECMWF spectral model (A. Beljaars 2001, personal communication). The UWM/COADS stresses are in good agreement with SOC in regions of moderate wind stress forcing but tend to be weaker for stresses greater than about 0.05 N m^{-2} , this difference is consistent with the lower values for C_{D10n} that were adopted for the UWM/COADS analysis at high wind speeds.

The differences discussed above are relatively minor when we consider the HR stresses which are persistently stronger than SOC and the other climatologies from the Tropics to mid latitudes. A measure of this difference is given by the annual mean wind stress magnitude averaged over the region from 45°S to 45°N , which for HR is 0.070 N m^{-2} compared with 0.057 N m^{-2} for SOC. The HR values are thus 23% larger than SOC on average, which is to be expected given the differences in the drag coefficient discussed in the preceding section and the conclusions of Harrison. At mid–high latitudes in the Northern Hemisphere the simple scaling between SOC and HR breaks down as a result of differences in gyre structure, which we investigate further in the next section.

To conclude this section, we briefly consider the characteristics of the fields in the Southern Ocean with the

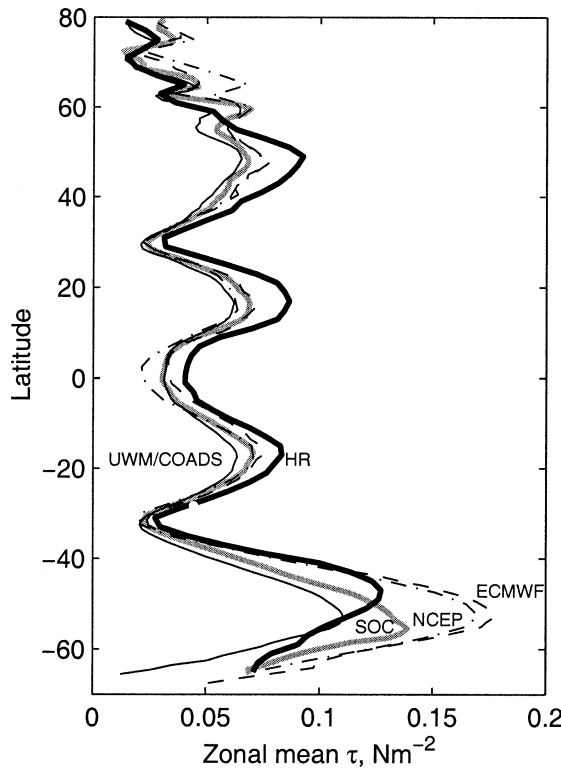


FIG. 5. Zonally averaged annual mean wind stress magnitude, units N m^{-2} . Solid gray line: SOC; solid thick black line: HR; solid thin black line: UWM/COADS; dashed black line: ECMWF; dash-dot line: NCEP–NCAR.

caveat that, as it contains very few in situ observations, we attach little significance to differences between the ship-based climatologies in this region. It is likely that the reanalyses provide better estimates of the stress in the Southern Ocean than the ship-based studies. We note that ECMWF and NCEP–NCAR show reasonable quantitative agreement and are typically stronger than the observation-based fields by about 40% in the band of maximum wind stress at $50^{\circ}\text{--}55^{\circ}\text{S}$ (see Fig. 5). This result is to be expected as the ship-based fields are likely to be strongly affected by the sparse data coverage in this region and reflect weaker wind forcing conditions in the more heavily sampled regions farther north. We note that comparisons with satellite-retrieved wind stresses have also indicated that ship-based products are biased low in the Southern Ocean (e.g., Chelton et al. 1990).

b. Impact of differences between SOC and HR on the wind driven response of the ocean

1) DIFFERENCES IN SOC AND HR SUBPOLAR GYRE STRUCTURE

The simple scaling between the HR and SOC stresses breaks down at mid–high latitudes, and here we find differences with respect to HR that were not noted by

Harrison. Despite the broad agreement in the positioning of the main features there are significant differences in their structure between HR and SOC, in particular for the subpolar gyres in the North Atlantic and North Pacific. These differences are most evident in the winter months: see the climatological mean fields for January for the two Northern Hemisphere basins shown in more detail in Figs. 6 and 7. In the North Atlantic, the subpolar gyre has stronger curvature and more intense central stresses in the SOC analysis than in HR. The scalar mean wind stress within a region centered on the gyre ($59^{\circ}\text{--}65^{\circ}\text{N}$, $30^{\circ}\text{--}40^{\circ}\text{W}$) is 0.17 N m^{-2} in SOC compared with 0.11 N m^{-2} for HR. In addition the forcing of the Greenland/Iceland/Norwegian Seas is stronger in SOC. In the North Pacific, the SOC stresses are stronger than HR in the latitude band, $50^{\circ}\text{--}60^{\circ}\text{N}$ and the structure of the subpolar gyre is different. Two distinct cyclonic gyres are evident in the HR field centered at (53°N , 175°E) and (57°N , 140°W) while in SOC there is a single basinwide subpolar gyre centered at (52°N , 160°W). Harrison did not discuss differences in subpolar gyre structure between his analysis and HR beyond noting that north of 55°N the close degree of correspondence between the pressure patterns broke down. Inspection of his Figs. 8–9, which shows the wind stress curl in January, indicates that he obtained a stronger double-gyre structure than HR in the North Pacific in contrast to our results. In the North Atlantic, it is not possible to draw firm conclusions on the strength of the subpolar gyre in his analysis as his presented fields terminate at 60°N , that is, south of the gyre center.

We note that sampling issues are of concern when analyzing the climatological fields. The number of ship reports tends to decrease at high latitudes in the North Atlantic (see, e.g., Fig. 2 of Josey et al. 1999) with the potential to generate sampling problems in determining the subpolar gyre structure. Fortunately, the gyre is centered on a region of greater than average sampling frequency at that latitude. The typical number of reports used to form the climatological monthly mean is of order 10–20 per $1^{\circ} \times 1^{\circ}$ grid cell in this area. This is similar to the frequency of observations at the sites of several of the subduction buoys, for which reliable stress determinations were obtained. Hence, it should be possible to obtain useful monthly mean wind stress estimates in the North Atlantic subpolar gyre although this issue is complicated by the stronger wind stress variability expected in the latter region. In this regard, we note in advance that results presented later in section 3c show good agreement between the SOC and NCEP–NCAR subpolar gyre wind stress variations indicating that month to month variability in this region is captured by the SOC dataset. Finally, we note that the sampling rate for the North Pacific subpolar gyre is somewhat higher than that in the North Atlantic, typically greater than 25 reports per $1^{\circ} \times 1^{\circ}$ grid cell, as it is crossed by one of the main shipping lanes.

Given the variation in period on which the SOC and

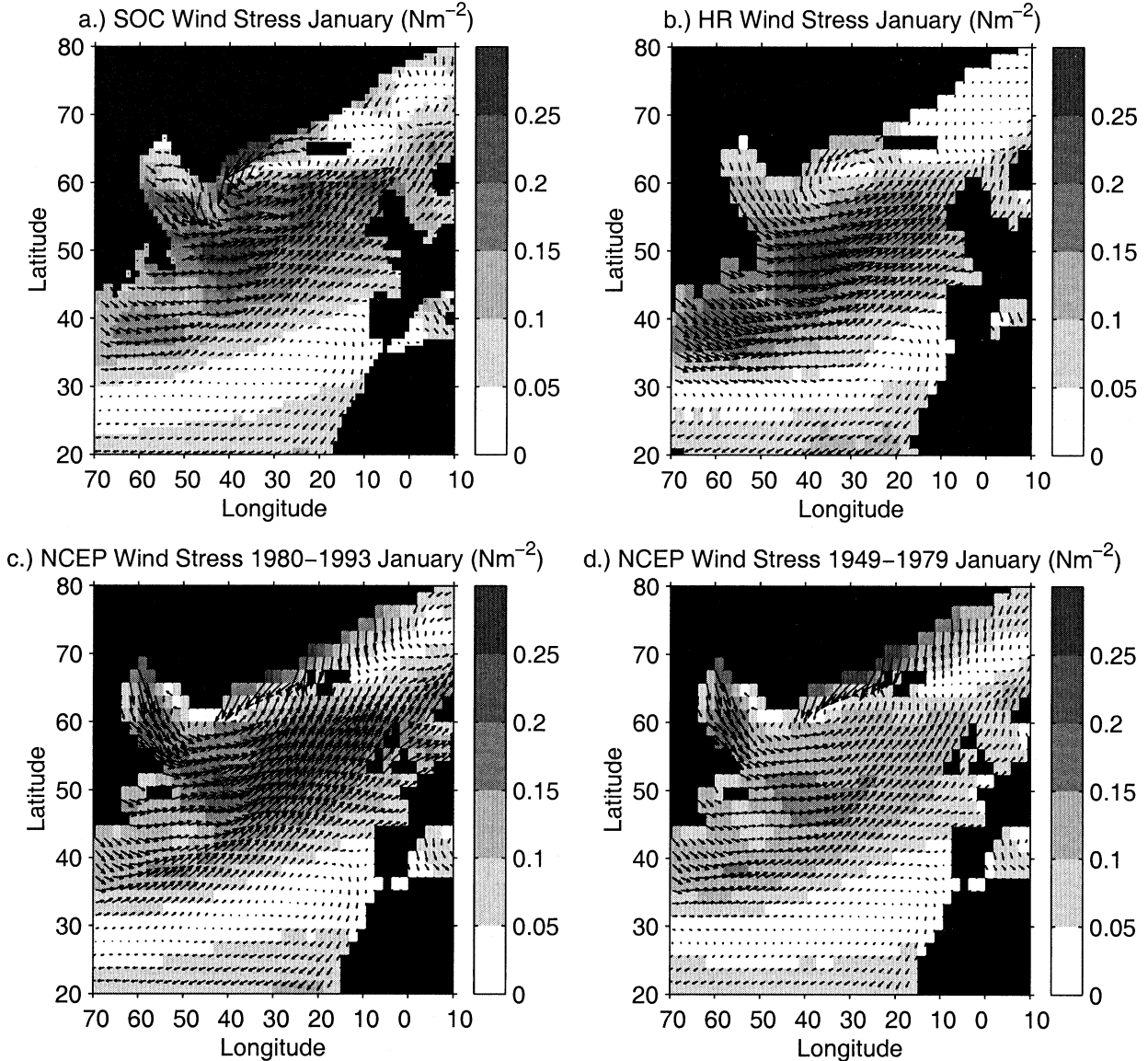


FIG. 6. Climatological mean fields for Jan of the wind stress in the mid-high latitude North Atlantic: (a) SOC, (b) HR, (c) NCEP 1980–93, and (d) NCEP 1949–79. Units N m^{-2} .

HR climatologies are based, the difference in the transfer coefficient schemes employed and the potential influence of variations in the sampling density of ship observations between the two analyses, it is difficult to directly attribute the observed differences in subpolar gyre structure to a single cause. Oscillations in the dominant large-scale pressure patterns in each of the Northern Hemisphere basins are known to occur on timescales longer than decadal (e.g., Hurrell and van Loon 1997; Mantua et al. 1997). Hence, we expect variations in the gyre structure between SOC and HR to arise in part as a result of the differences in the period on which each is based. The SOC fields were generated from ship reports within the period 1980 to 1993 and will thus reflect the dominant pressure patterns in this interval. The HR

fields are based on a much longer interval (1870–1976) and hence represent a mean over a number of oscillations. Between 1980 and 1993, the North Atlantic Oscillation (NAO) index was predominantly positive (Hurrell and van Loon 1997) favoring a strong Icelandic low; hence the stronger subpolar gyre in SOC relative to HR is to be expected. Further support for the increase in strength of the subpolar gyre in recent decades is provided by an additional study of the NCEP–NCAR fields, which were produced with a fixed analysis system. The fields have been subsetted on the intervals 1949–79 and 1980–93, for which January mean wind stress fields are shown in Figs. 6c–d. Over the period 1980–93 the subpolar gyre in NCEP–NCAR is significantly stronger and has tighter curvature than in the preceding decades.

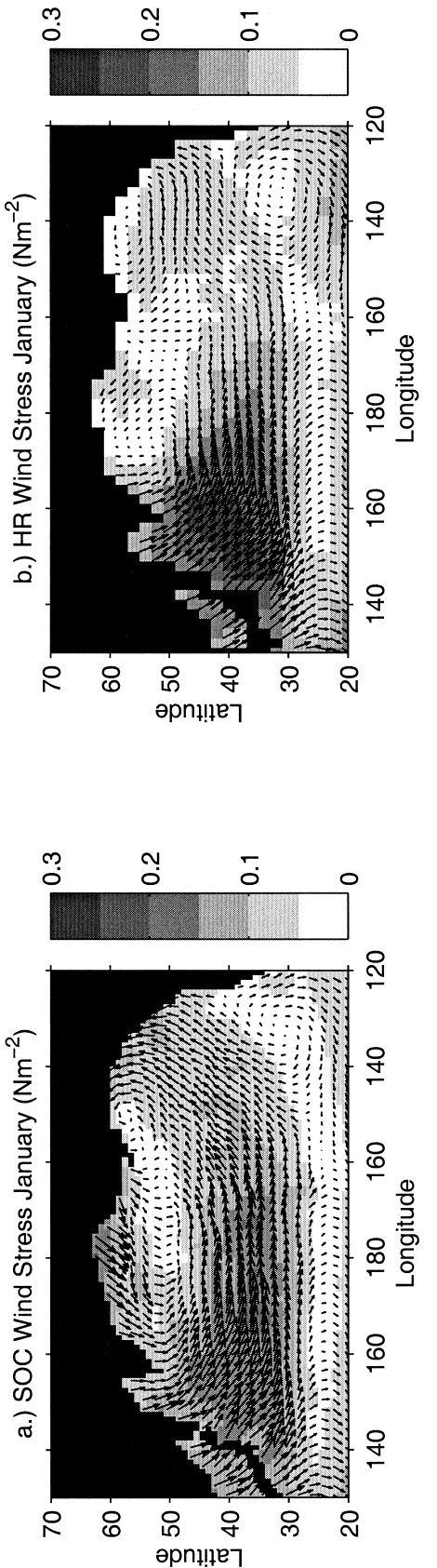


FIG. 7. Climatological mean fields for Jan of the wind stress in the North Pacific: (a) SOC, (b) HR. Units N m^{-2} .

The primary mode of pressure variation in the North Pacific, variously termed the North Pacific Oscillation (Gershunov and Barnett 1998) or Pacific Decadal Oscillation (Mantua et al. 1997), also tended to be in a positive state during the period used to form the SOC climatology. This state is characterized by a deepening and eastward shift of the Aleutian low, which is evident in the comparison of the SOC fields and HR. Trenberth et al. (1990) found similar changes in the wind stress field in the North Pacific relative to HR in their analysis of ECMWF model output for the period 1980–86.

2) EKMAN TRANSPORT

The response of the upper-layer ocean circulation to wind forcing is described by Ekman transport theory (e.g., Gill 1982). The wind-driven zonal, E_x , and meridional, E_y , Ekman volume transports across the sides of a given grid cell are given by

$$E_x = (f\rho_w)^{-1}L_y\tau_y \quad (5a)$$

$$E_y = -(f\rho_w)^{-1}L_x\tau_x, \quad (5b)$$

where $f = 2\Omega \sin\varphi$ is the Coriolis parameter, with $\Omega = 7.20 \times 10^{-5} \text{ s}^{-1}$ and φ the latitude; ρ_w , the density of sea water in the Ekman layer, assumed to be 10^3 kg m^{-3} ; L_x and L_y , the zonal and meridional dimensions of the cell. In our analysis, the following approximate values for $L_x = 1.11 \times 10^5 \cos\varphi \text{ m}$ and $L_y = 1.11 \times 10^5 \text{ m}$ have been adopted for a $1^\circ \times 1^\circ$ grid cell.

Estimates of the monthly mean Ekman transport have been obtained from the SOC wind stress fields using (5a–b) and compared with HR. The variation of the zonally integrated meridional transport for each of the major ocean basins is shown in Fig. 8, where the units are Sverdrups ($\text{Sv} \equiv 10^6 \text{ m}^3 \text{ s}^{-1}$) and positive values imply a northward transport. Our results are similar to those of Harrison in that the choice of a smaller drag coefficient for the SOC wind stress typically leads to estimates of the Ekman transport that are smaller in magnitude than HR by about 25%. The differences in gyre structure noted in the preceding section do not lead to large differences in the Ekman transport as the increase in f with latitude results in relatively small values for the transport at mid–high latitudes. Note the difference in direction (equatorward) of the Ekman transport in the tropical Indian Ocean north of the equator compared to the poleward transport found in the other basins at these latitudes. This difference reflects the dominance of the southwest Monsoon in the annual mean in the Indian Ocean.

Values for the Ekman transport from HR and SOC across several recent oceanographic sections are listed in Table 3. It is in the Tropics that the Ekman transport becomes significant, and differences between the various climatological estimates may lead to large uncertainties in hydrographic estimates of the total volume

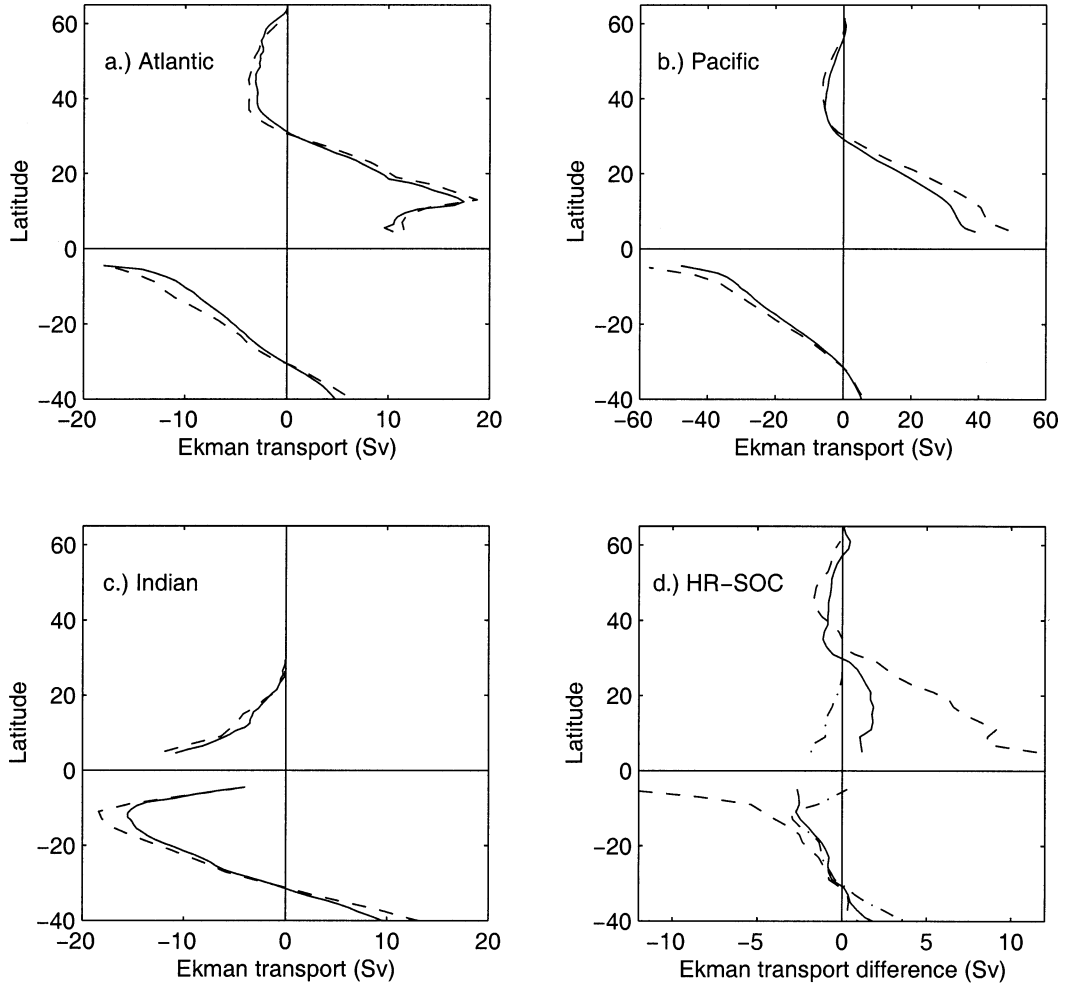


FIG. 8. Zonal annual mean northward Ekman transport in (a) the Atlantic, (b) Pacific, and (c) Indian Oceans for the SOC (solid line) and HR (dashed) climatologies. (d) The difference (HR - SOC) of the northward Ekman transport for the Atlantic (solid line), Pacific (dashed), and Indian (dash-dot) Oceans. Units are Sv.

and heat transports. At 10°N in the Pacific, there is a difference of 8.6 Sv in the estimates of 32.6 Sv and 41.2 Sv obtained from SOC and HR. To put this in context, Wijffels et al. (1996) find in an analysis of a

hydrographic section at this latitude that an uncertainty of 6 Sv in the Ekman transport results in an additional error of 0.4 PW (1 PW = 10^{15} W) in the heat transport across the section. The value of 37 Sv that they adopted following an analysis of The Florida State University pseudostresses and other available estimates lies between SOC and HR. Use of the SOC value would reduce their estimate of the poleward heat transport across this section by 0.3 PW from 0.7 to 0.4 PW.

In the tropical Atlantic, Klein et al. (1995) analyzed hydrographic sections at 8° and 14.5°N. For their analysis, they obtained Ekman transport estimates from the Isemer and Hasse (1987) climatology of 15.2 Sv and 13.6 Sv respectively, which implied an Ekman convergence of 1.6 Sv in the region between the sections. In contrast, both the SOC and HR estimates imply a divergence from this region of 5 Sv, primarily as a result of the estimate at 8°N being smaller than that found by Isemer and Hasse (1987) by of order 4 Sv. The impact of these differences for the implied heat transport across

TABLE 3. Climatological annual mean Ekman transport across various zonal hydrographic sections from SOC and HR. Note that the 60°N North Atlantic section runs from Southern Greenland to Northern Scotland and is a zonal approximation to the section reported by Bacon (1997).

Hydrographic section	SOC Ekman (Sv)	HR Ekman (Sv)
10°N Pacific (Wijffels et al. 1996)	32.6	41.2
24°N Pacific (Bryden et al. 1991)	9.0	12.7
11°S Atlantic (Speer et al. 1996)	-9.6	-12.1
8°N Atlantic (Klein et al. 1995)	10.8	11.6
14.5°N Atlantic (Klein et al. 1995)	15.8	16.6
24°N Atlantic (Hall and Bryden 1982)	6.3	7.2
60°N Atlantic (Bacon 1997)	-1.3	-1.5
32°S Indian (Bryden and Beal 2001)	0.6	1.1

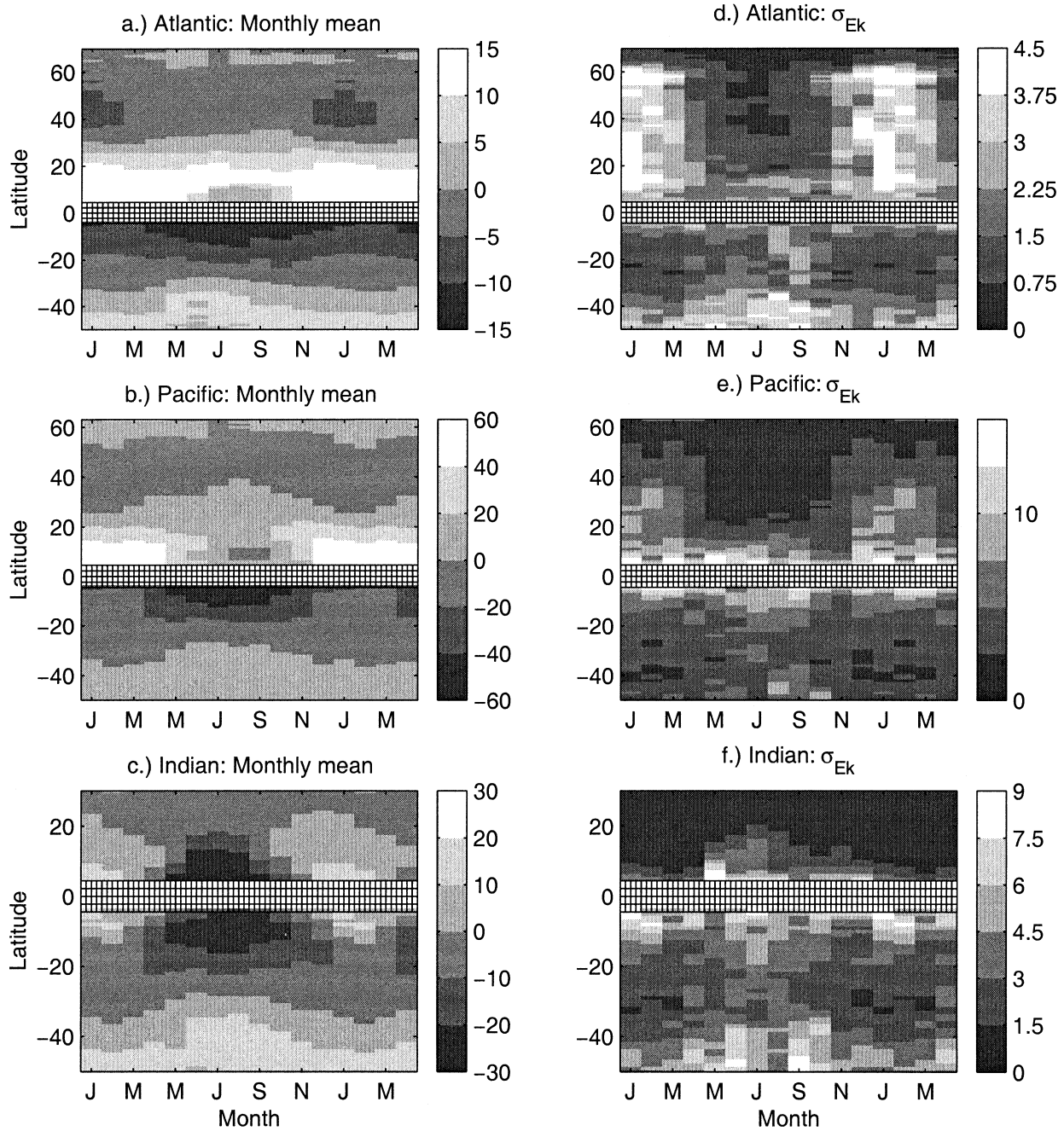


FIG. 9. Seasonal variation of SOC climatological monthly mean northward Ekman transport with latitude in (a) the Atlantic, (b) Pacific, and (c) Indian Oceans. (d)–(f) The interannual variability within the period 1980–93 for each month, as measured by the standard deviation of the individual monthly values σ_{Ek} . Units are Sv. The cross-hatched area excludes the band from 4°S to 4°N for which transport values were not calculated.

the two sections is not clear as the inverse analysis of the paired section data carried out by Klein et al. (1995) would have to be repeated.

The differences between the climatological estimates are less significant at higher latitudes. At 24°N in the North Atlantic, the SOC and HR Ekman transport estimates differ by just 0.9 Sv. In the North Pacific at

24°N, the difference is somewhat larger by virtue of the basin width, with estimates of 9.0 Sv from SOC and 12.7 Sv from HR; similar figures are obtained at 11°S in the Atlantic while for the other two sections tabulated the differences are less than 1 Sv.

In addition to the uncertainty arising from the choice of climatology, significant differences in hydrographic

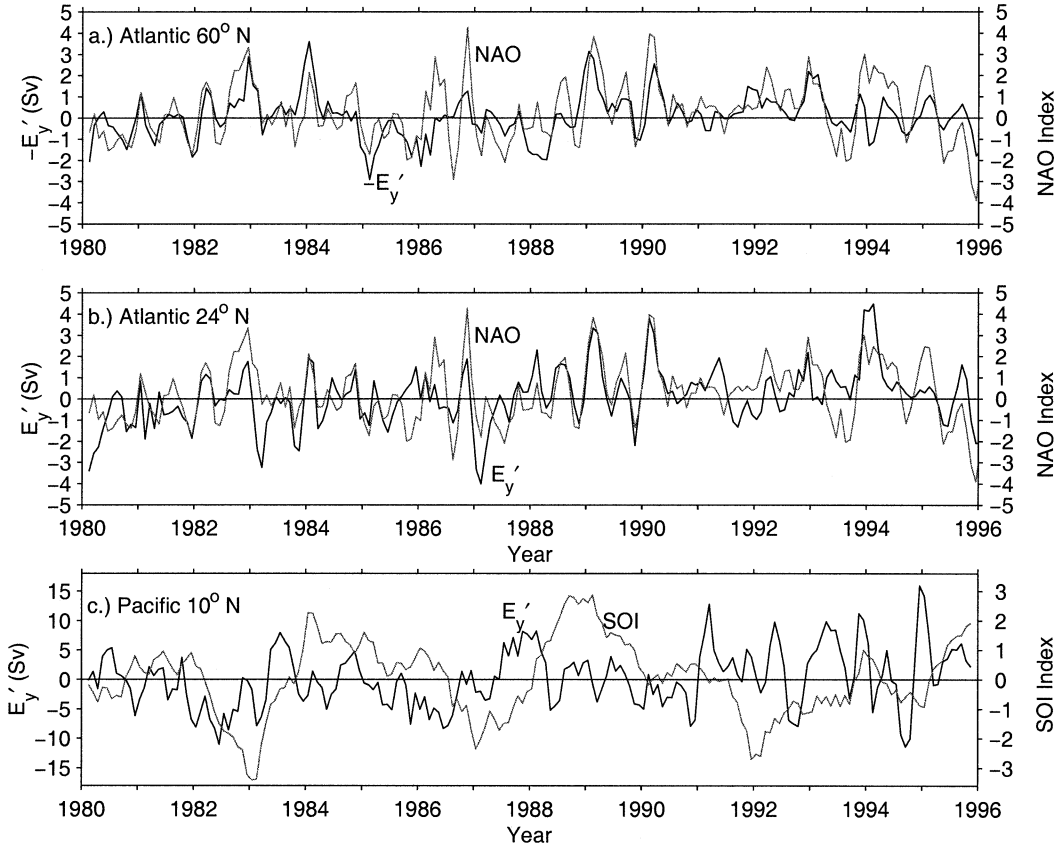


FIG. 10. Time series of the anomalous meridional Ekman transport (E_y' , units Sv), determined from the SOC climatology, across various hydrographic sections: (a) 60°N Atlantic, (b) 24°N Atlantic, and (c) 10°N Pacific. Also shown are time series of the NAO index and SOI. Note that all time series have been smoothed with a 3-point running mean and that the 60°N transport has been multiplied by -1 .

estimates of the ocean heat transport may arise depending on whether climatological Ekman transport estimates or values obtained from the observed wind field at the time of the cruise are employed. For example, Klein et al. (1995) have discussed the effects of variability with regard to estimates of the heat transport across 8° and 14.5°N in the Atlantic. They find values of 1.18 and 1.22 PW across these two sections if climatological stresses are used compared with 1.69 and 1.37 PW if the observed winds are employed.

Analysis of the SOC dataset indicates that significant interannual variability in the Ekman transport occurs over a range of latitudes. The interannual variability in each major basin has been quantified by calculating the standard deviation σ_{Ek} of the zonally integrated meridional Ekman transport (where the sample consists of the 14 individual values for each calendar month within the period 1980–93). The variation of the climatological monthly mean meridional Ekman transport and σ_{Ek} with latitude for each of the major ocean basins is shown in Fig. 9. In the Atlantic and Pacific Oceans, the Ekman transport is directed poleward on either side of the equator throughout the year. In the Indian Ocean, the seasonal variation is somewhat different with southward

transport on both sides of the equator during summer and northward transport in winter. The strongest interannual variability in the North Atlantic occurs at mid-high latitudes in winter. At $40^\circ\text{--}50^\circ\text{N}$, σ_{Ek} is of the same magnitude, 5 Sv, as the climatological mean value. In the other basins, interannual variability is dominated by variations close to the equator, although it can also be significant at higher latitudes, σ_{Ek} being greater than 10 Sv at 30°N in the Pacific in February.

The relationship between the Ekman transport variability across several latitudes that correspond to recent hydrographic sections and the major atmospheric pressure oscillations has been investigated. Time series of the anomalous (i.e., with the seasonal cycle removed) Ekman transport across hydrographic sections at 24° and 60°N in the Atlantic and 10°N in the Pacific, and of the NAO and Southern Oscillation are shown in Fig. 10; each series has been smoothed with a 3-point running mean. The NAO index is that defined by Hurrell (1995) while the Southern Oscillation index has been determined from reported surface pressures in the SOC dataset averaged over regions centered on Tahiti and Darwin using the method of Zhang et al. (1997); see Josey (1999) for details. In the North Atlantic, variability in

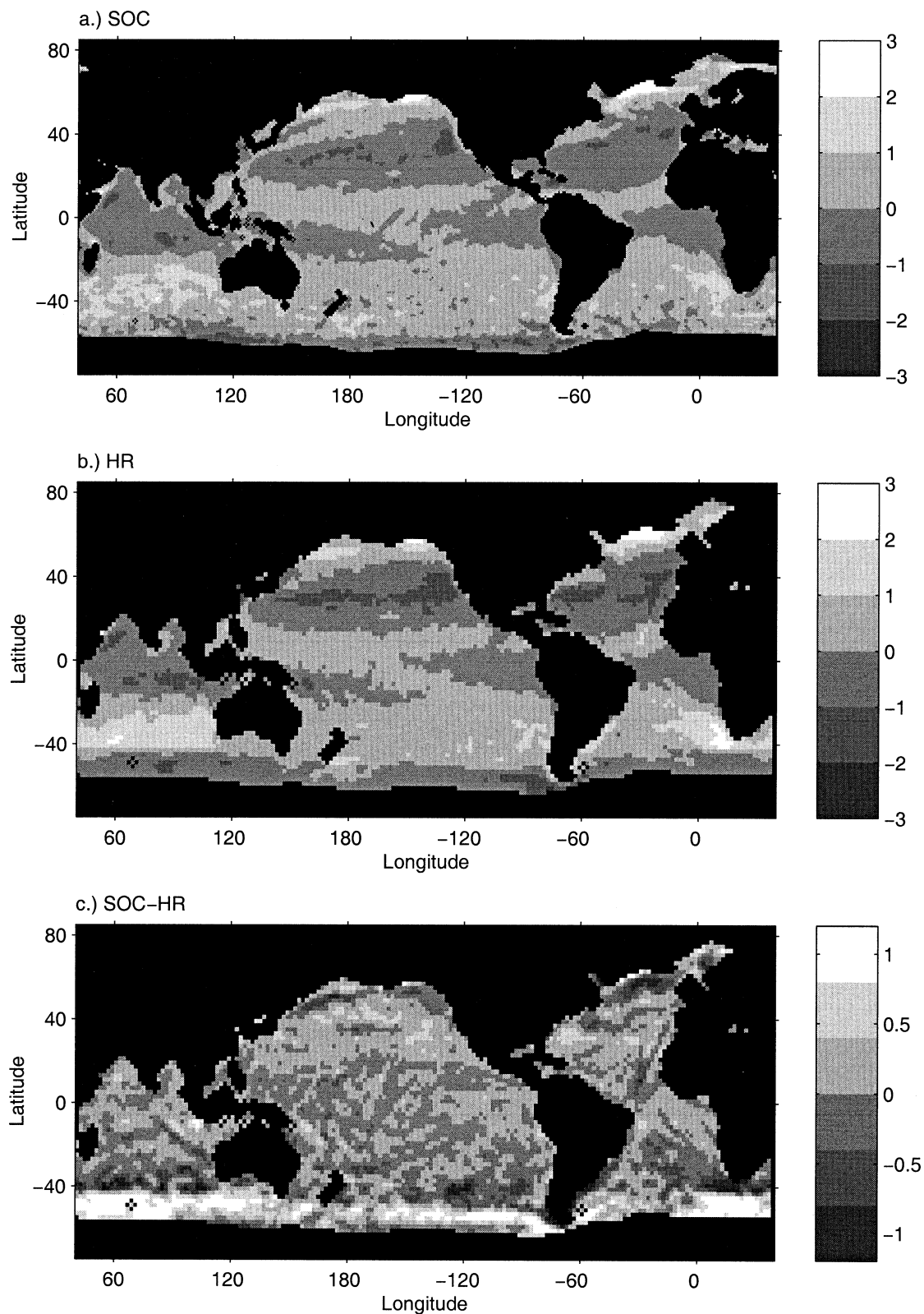


FIG. 11. Annual mean wind stress curl field for (a) SOC, (b) HR, and (c) SOC–HR. Units N m^{-3} .

the Ekman transport shows an in-phase correlation with the NAO at both 24°N ($r^2 = 0.34/0.58$ for all months/December–March; note that the r^2 values are for the time series before smoothing) and 60°N ($r^2 = 0.39/0.55$). This is to be expected as these sections lie to the south of the centers of the subpolar and subtropical gyres respectively, so the transport across them will reflect variations in the gyre strength caused in part by the NAO. High values for the NAO index reflect an increase in the strength of both gyres and thus a stronger southward/northward Ekman transport across 60°N/24°N. Note that the strength of the correlations increases if December–March only values are selected as the NAO signal tends to be stronger in winter (Hurrell 1995). In contrast, the transport across 10°N in the tropical Pacific is not in phase with the SOI but appears instead to lead it by about a year within the interval 1982–90. The peak correlation, $r^2 = 0.27$, occurs for a lead interval of 12 months; at zero lead the two time series are uncorrelated ($r^2 = 0.01$). We are aware of the dangers of interpreting short time series (Wunsch 1999) but note that the behavior within this interval indicates that an integral measure of the ocean response to the wind stress field may provide a useful predictor for the Southern Oscillation.

To conclude this section, we stress that an inappropriate choice of Ekman transport can lead to large errors in derived ocean transports in the Tropics. In particular, use of HR in the tropical Pacific gives rise to differences of order 10 Sv with respect to SOC.

3) WIND STRESS CURL AND EKMAN PUMPING

In this section, we discuss the wind stress curl and consequent vertical Ekman response of the ocean, the focus being on the effects of differences in the subpolar gyre structure between SOC and HR noted earlier on the exchange of water between the Ekman and lower layers in winter. Climatological mean fields of the winds stress curl,

$$\text{curl}_z \boldsymbol{\tau} = \frac{\partial \tau_y}{\partial x} - \frac{\partial \tau_x}{\partial y} \quad (6)$$

have been calculated using a simple centered finite difference scheme following Saunders (1976). Denoting the latitude and longitude of a given cell by indices (i, j) ,

$$\begin{aligned} \text{curl}_z \boldsymbol{\tau}(i, j) &= \frac{\tau_y(i+1, j) - \tau_y(i-1, j)}{2L_x} \\ &\quad - \frac{\tau_x(i, j+1) - \tau_x(i, j-1)}{2L_y}. \end{aligned} \quad (7)$$

The annual mean wind stress curl fields for SOC and HR and their difference are shown in Fig. 11. The main features of the field are qualitatively similar to those found by HR and Harrison; the structure being primarily zonal with alternate bands of positive and negative cur-

vature. From the Tropics to midlatitudes the magnitude of the wind stress curl tends to be smaller in SOC than HR by about 20% as a result of the lower drag coefficient. Note that Fig. 11c is somewhat noisy and that the difference between SOC and HR is more easily seen in the Sverdrup transport, to be discussed in section 3e, as the latter provides an integral measure of the curl field.

Curvature of the wind stress field leads to convergence (or divergence) of the wind-driven transport in the Ekman layer and downwelling (upwelling) of water, commonly termed Ekman pumping (suction). Whether downwelling or upwelling occurs depends on the signs of the curvature and Coriolis parameter, the Ekman velocity of the vertical motion being given by the following equation (e.g., Gill 1982),

$$w_e = (f\rho_w)^{-1} \text{curl}_z \boldsymbol{\tau}. \quad (8)$$

Climatological monthly mean fields of w_e have been determined using (8).

In the mid-high latitude North Atlantic and North Pacific basins in winter, the variations in gyre structure between HR and SOC have interesting consequences for the vertical Ekman exchange. Plots of w_e for January in SOC and HR for each basin are shown in Fig. 12. In the North Atlantic, Ekman upwelling velocities associated with the subpolar gyre in winter are noticeably stronger and confined to a smaller area in the SOC analysis than obtained from HR. This is to be expected given the stronger curvature of the gyre in SOC noted earlier. Enhanced upwelling in the Nordic seas and weaker upwelling over the region to the south of the subpolar gyre is also noticeable in the SOC field when compared with HR.

The difference in upwelling in the subpolar gyre region has been quantified by taking an area average of the January mean vertical velocity in the box (59°–65°N, 30°–40°W). A value of $7.3 \times 10^{-6} \text{ m s}^{-1}$ is obtained for the SOC field compared with $3.3 \times 10^{-6} \text{ m s}^{-1}$ for HR. Expressed as a monthly rate, the difference between the two climatological values amounts to an additional Ekman suction of $10.3 \text{ m month}^{-1}$ in January, the SOC and HR values being 18.9 and 8.6 m month^{-1} , respectively. Part of this difference might be expected to be due to the difference in grid scale between the two climatologies. Saunders (1976) has noted that the strength of the wind stress curl may increase as the grid scale is reduced. Repeat calculation of the SOC curl using the January means averaged onto a $2^\circ \times 2^\circ$ grid leads to only minor changes of order 10% in w_e , the subpolar gyre box mean value being reduced to $6.5 \times 10^{-6} \text{ m s}^{-1}$. This indicates that the differences in upwelling rate between SOC and HR are not due to the choice of grid although the picture is complicated somewhat by the effect of the smoothing procedure in each analysis on the resolution; see the discussion in Kent et al. (2000).

In the North Pacific, the w_e field has a more complex spatial dependence than the North Atlantic, the regions

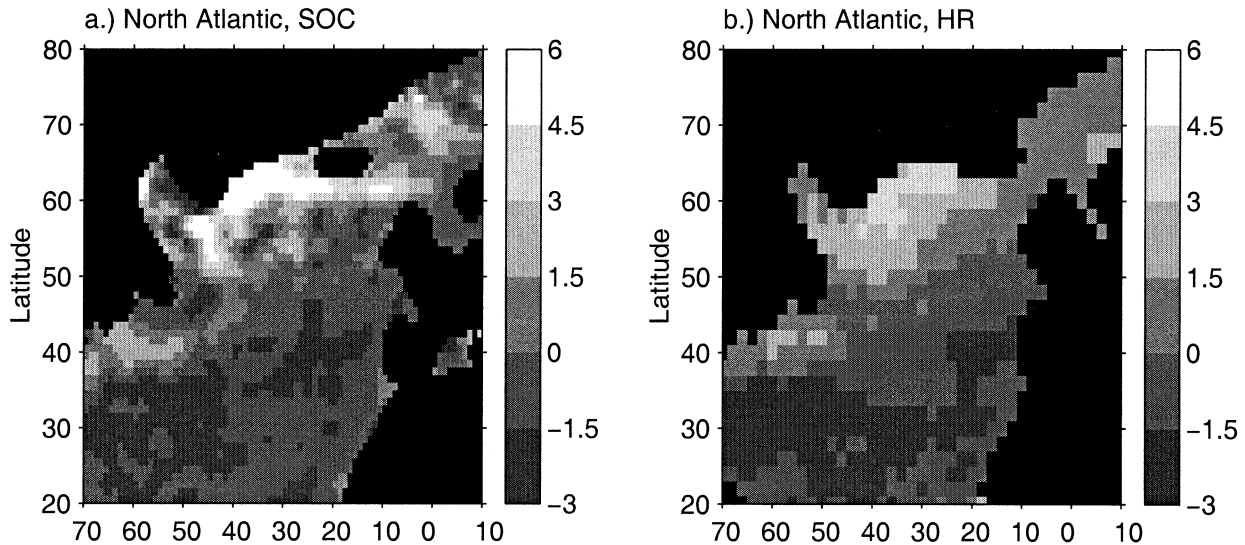


FIG. 12. January mean Ekman vertical velocity in the North Atlantic for (a) SOC and (b) HR, and North Pacific for (c) SOC and (d) HR. Units 10^{-6} m s^{-1} .

of strongest upwelling in HR are centered on the two gyres noted in section 3a, the gyre in the northwest of the basin dominates with peak values of order 4.5 m s^{-1} . For SOC, there are a number of regions of strong upwelling with generally greater Ekman suction in the centre of the basin at midlatitudes than HR.

4) SVERDRUP TRANSPORT

As discussed in the introduction, there has been considerable debate over the significance of the Sverdrup transport ψ_s . For completeness, we compare annual mean fields of ψ_s derived from the SOC and HR climatologies. We regard these as providing a useful indicator of the integrated atmospheric forcing of the ocean but are aware that ψ_s may not accurately reflect the true ocean circulation. Hence, we do not attempt to draw any inferences regarding the relative merits of the two climatologies by comparing the derived transports with measured currents. The transport has been determined by integrating zonally from a boundary value of zero at the eastern margin x_E of each of the major ocean basins to a given longitude x_W according to the following equation (e.g., Gill 1982):

$$\psi_s = (\partial f / \partial y)^{-1} \int_{x_E}^{x_W} \text{curl}_z \boldsymbol{\tau} dx. \quad (9)$$

Fields of ψ_s are shown in Fig. 13. At the western boundary in each of the major basins values from HR are typically stronger than SOC by 20%–30%, reflecting the generally stronger curl field arising from the larger drag coefficient. The most noticeable differences occur in the western Pacific where values of 49 and 39 Sv, respectively, for SOC and HR are obtained off the southern tip of Japan ($26^\circ\text{N}, 130^\circ\text{E}$). At a location (26°N ,

78°W) close to the Straits of Florida the respective Sverdrup transports for HR and SOC are 25 and 20 Sv.

c. The influence of the NAO on the Ekman response of the North Atlantic

We have noted that the stronger upwelling rate in the high latitude North Atlantic in SOC relative to HR is consistent with the predominantly positive state of the NAO within the period used to generate the SOC fields. Here we quantify the influence of the NAO on the vertical Ekman response of the ocean using the SOC dataset. A composite plot of the difference in mean Ekman vertical velocity between the five winters (December–March) with the highest Hurrell NAO index and the five lowest index winters in the period 1980–97 is shown in Fig. 14. The selected winters and the index value for each are listed in Table 4. The increase in magnitude of the subpolar gyre upwelling/subtropical gyre downwelling rates between the two extremes of the NAO is evident, the difference in the region to the southwest of Iceland being of order $3 \times 10^{-6} \text{ m s}^{-1}$ (equivalently 7 m month^{-1}). We note that a similar pattern (not shown) is obtained if a composite is formed on individual winter months, and in the latter case the extreme upwelling/downwelling velocities are stronger by a factor of ~ 2 as a greater range of NAO index values are sampled.

The degree to which changes in the net vertical exchange of water across the base of the Ekman layer in the two gyres can be accounted for by variations in the NAO has been investigated by calculating integrated volume fluxes for boxes spanning each gyre. The following boxes have been employed: subpolar gyre (58° – 70°N , 45° – 0°W)/subtropical gyre (20° – 50°N , 50° – 10°W). The seasonal cycles of the volume flux in each gyre and the difference,

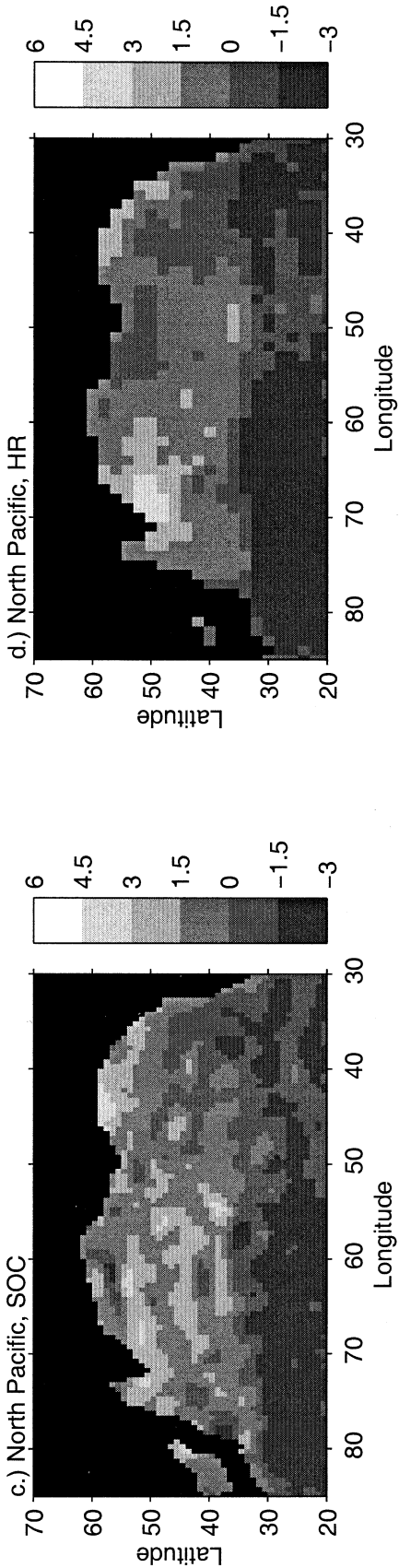


FIG. 12. (Continued)

$$\Delta V = V_{SP} - V_{ST}, \quad (10)$$

where V_{SP} and V_{ST} are the volume fluxes for the subpolar and subtropical gyres, respectively, are shown in Fig. 15a. For each gyre, the amplitude of the seasonal cycle is about 4 Sv, peaking in winter, leading to a variation of order 8 Sv in ΔV .

Time series of the anomalous (i.e., with the seasonal cycle removed) volume flux in the two gyres, V'_{SP} and V'_{ST} and their difference, $\Delta V'$, together with the NAO index are shown in Fig. 15b. There is a clear correlation between variations in the NAO and the vertical volume flux in each gyre. The relationship is slightly stronger for the subpolar gyre than the subtropical, $r^2 = 0.43/0.38$ for the correlation of the NAO with V'_{SP}/V'_{ST} . Considering the difference in the volume flux in each gyre, we find $r^2 = 0.51$ for the correlation of the NAO index with $\Delta V'$. Thus, more than half of the variance in the main ocean gyre upwelling and downwelling rates in the North Atlantic as characterized by $\Delta V'$ can be explained by the leading atmospheric mode of sea level pressure variability. Note that the NAO is more strongly correlated with $\Delta V'$ than with V'_{SP} or V'_{ST} . This is to be expected since the NAO measures the relative strength of the sea level pressure in the two gyres. Further, if the comparison is restricted to winter (Dec–Mar) months, r^2 increases in value from 0.51 to 0.64. The impact of the NAO on the vertical exchange has been quantified by linearly regressing $\Delta V'$ on the NAO; a unit increase in the index leads to an increase in $\Delta V'$ of $1.5 \pm 0.2/2.1 \pm 0.3$ Sv (all months/Dec–Mar only).

In order to check that the relatively low sampling inherent in the ship-based SOC dataset has not significantly influenced our results we have repeated the above study with the NCEP–NCAR model reanalysis for which sampling is not such an issue. We obtain very similar results with the NCEP–NCAR fields (see Fig. 16). The correlation between the NAO and $\Delta V'$ is slightly stronger using NCEP–NCAR, $r^2 = 0.57/0.69$ (all months/Dec–Mar only). For NCEP–NCAR, unit increase in the NAO leads to an increase in $\Delta V'$ of $1.8 \pm 0.3/2.4 \pm 0.3$ Sv; which although slightly stronger than SOC is in agreement with the SOC values within the stated error range. We note in addition that the NCEP–NCAR and SOC $\Delta V'$ time series show a very strong correlation, $r^2 = 0.84$, with the same value being obtained for both the full year and winter only datasets. The high level of correlation between NCEP–NCAR and SOC indicates that the relatively low sampling rate is not a major problem when using the SOC dataset to evaluate the wind-driven forcing of the ocean at gyre scales in the North Atlantic.

4. Conclusions

We have presented an evaluation of the Southampton Oceanography Centre (SOC) climatology wind stress fields that has considered their accuracy with respect to

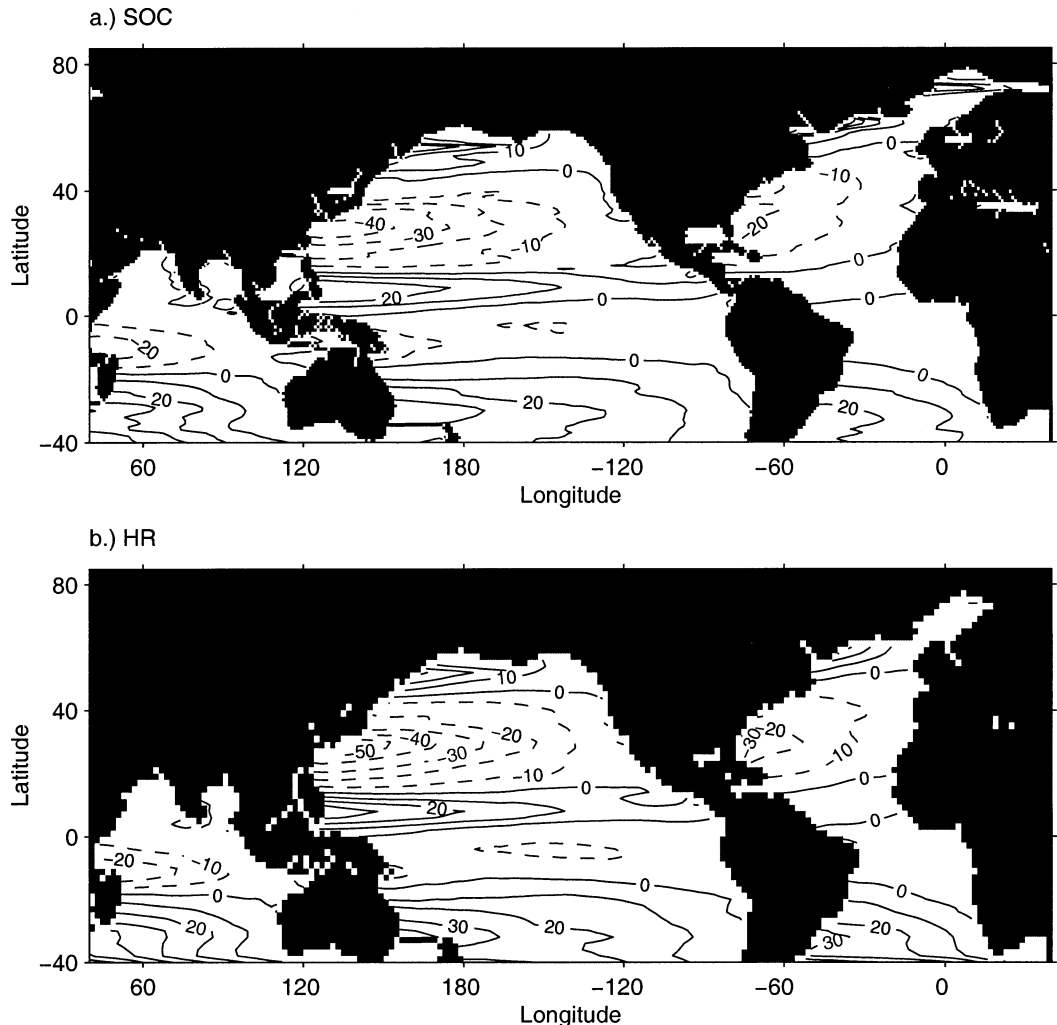


FIG. 13. Annual mean Sverdrup transport for (a) SOC and (b) HR. Units are Sv. Contour interval 10 Sv; negative contours dashed.

research buoy measurements together with how they compare with other ship-based climatologies and fields from the atmospheric model reanalyses. The most significant differences are those between SOC and the widely used Hellerman and Rosenstein (HR) climatology and the effect of these differences on the wind-driven response of the ocean have been investigated at length. In addition, we have examined the role of the NAO in driving variability of Ekman pumping and suction in the North Atlantic using both SOC and NCEP–NCAR. Our focus has been on the mid–high latitudes and we have not discussed in detail the characteristics of the wind stress fields in the Tropics.

The accuracy of the SOC stresses has been assessed

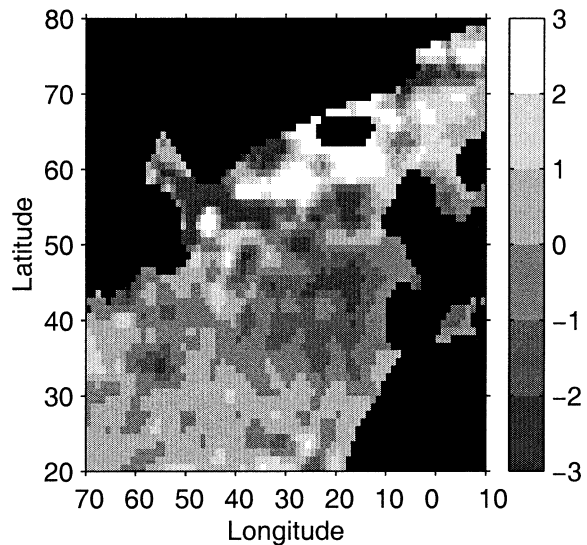


FIG. 14. Difference in SOC composite mean North Atlantic Ekman vertical velocity between the five most extreme NAO+ and NAO– winters in the period 1980–97. Units are 10^{-6} m s^{-1} .

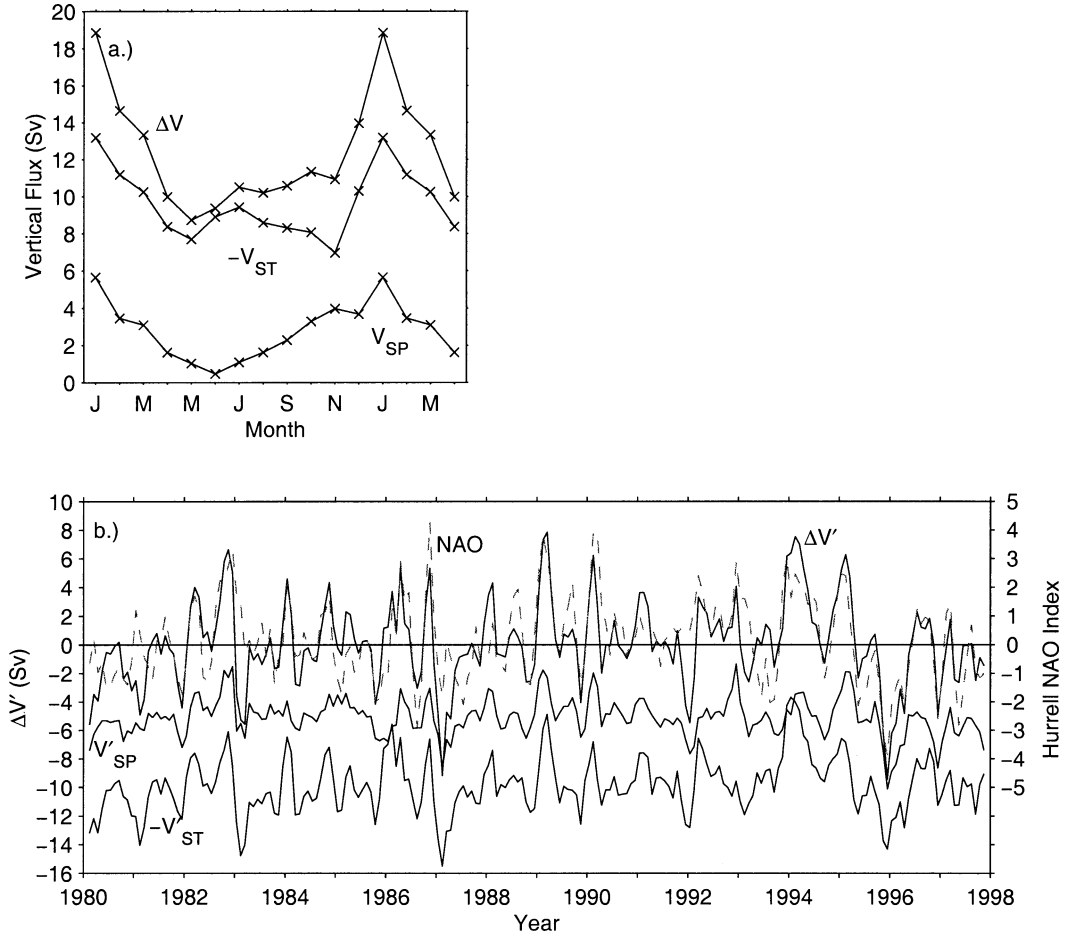


FIG. 15. (a) SOC climatological seasonal cycle in the vertical Ekman fluxes across the subpolar (V_{SP}) and subtropical (V_{ST}) gyres, and their difference (ΔV), units Sv. Note that the subtropical gyre flux has been multiplied by -1 ; (b) time series of the SOC anomalous volume flux in the subpolar gyre V'_{SP} (offset by 5 Sv), subtropical gyre V'_{ST} (multiplied by -1 and offset by 10 Sv), the anomalous volume flux difference ($\Delta V'$), and the Hurrell NAO index (dashed line).

at several locations by comparison of individual monthly means with collocated values from several Woods Hole IMET buoy deployments. Results for the Subduction Buoy array comparisons indicate that the random error in the SOC climatological monthly means typically ranges from 0.001 to 0.002 $N\ m^{-2}$ over much of the midlatitude Northern Hemisphere ocean basins. Reasonable agreement is also obtained for buoys deployed

TABLE 4. The five most extreme NAO+ and NAO- winters in the period 1980–97 as determined from the Hurrell (1995) NAO index. Winter is defined to run from Dec to Mar and the year listed refers to the year containing Jan-Mar.

NAO-		NAO+	
Winter	NAO index	Winter	NAO index
1985	-0.8	1983	1.9
1987	-0.7	1989	3.0
1988	-0.1	1990	2.0
1996	-2.4	1994	2.6
1997	-0.5	1995	2.4

in regions that are more sparsely sampled by ships, in particular the Arabian Sea for which the random error estimate is of order $0.004\ N\ m^{-2}$. We are limited in our error assessment by the availability of high-quality continuous time series of wind stress estimates from research buoys. Thus, we are not at present able to provide useful estimates of the wind stress error in the Southern Ocean, which has very low sampling. Given the extremely limited amount of in situ information available for such regions, we anticipate that fields from the reanalyses will prove to be more accurate in such regions. We note that there is no evidence from the comparisons with the various buoy observations that the SOC climatology systematically underestimates the wind stress. Thus, the suggestion that the low sampling rate inherent in ship-based stress estimates leads to them generally underestimating the true stress (e.g., Mestas-Nunez et al. 1994) is not supported by our analysis although we note again that we have not been able to test regions of extremely low sampling such as the Southern Ocean.

The large-scale characteristics of the SOC fields have

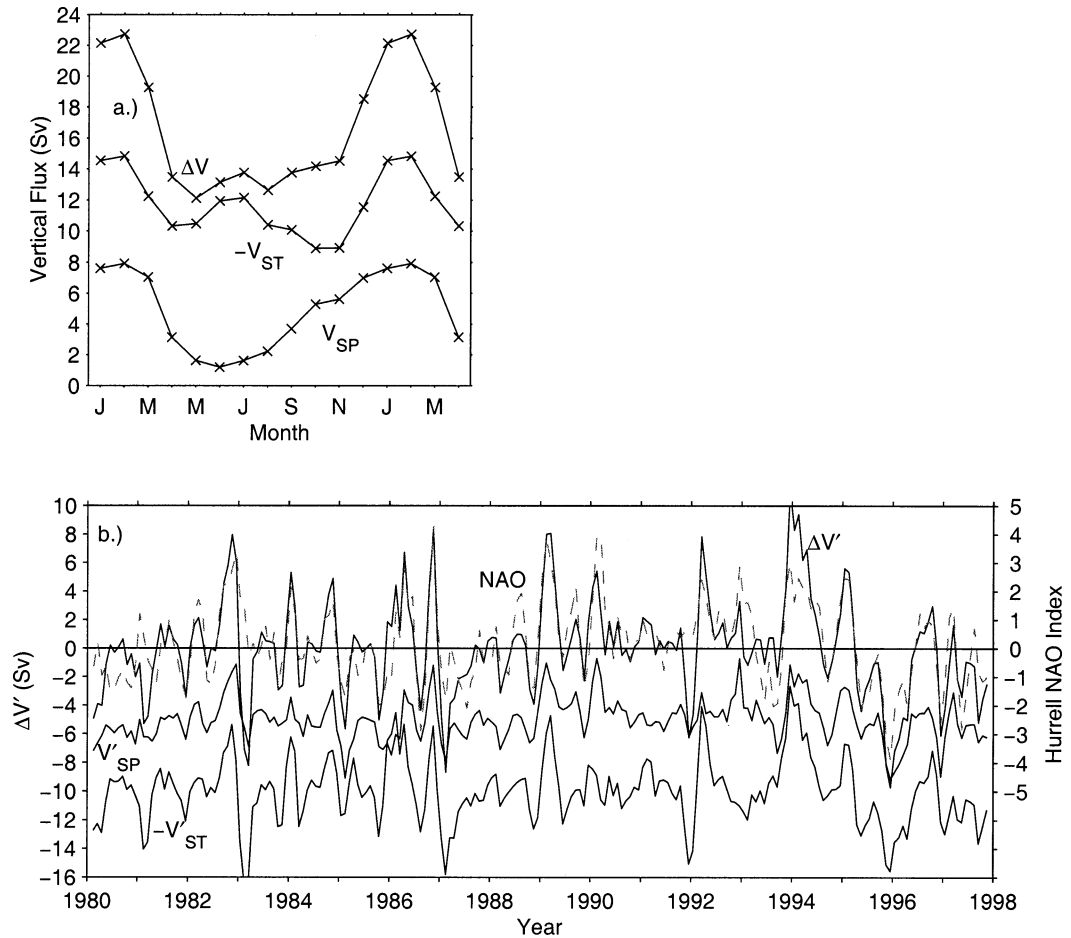


FIG. 16. As in Fig. 15 except that the vertical Ekman fluxes have been calculated using the NCEP–NCAR reanalysis.

been compared with those of the NCEP–NCAR and ECMWF atmospheric model reanalyses, and the in situ observation based UWM/COADS and Hellerman and Rosenstein (HR) climatologies. The NCEP–NCAR fields show noticeably weaker wind stress forcing in the Tropics than SOC while ECMWF and UWM/COADS are in good agreement. From the Tropics to the mid-latitudes, the HR stresses tend to be stronger than SOC and the other recent climatologies. At higher latitudes this simple scaling breaks down and differences in the spatial structure of the Northern Hemisphere subpolar gyres are found that are consistent with known variations in the state of the major atmospheric pressure oscillations. Intercomparison of the ship-based zonally averaged wind stress in the Southern Ocean with the reanalyses indicates that the SOC and other in situ based climatologies may significantly underestimate the forcing in this region as the reanalyses fields are stronger by up to 40%.

The North Atlantic subpolar gyre is more intense in the SOC analysis than HR, and we suggest that this difference is due to the predominantly positive state of

the NAO throughout the period used to formulate the SOC climatology. A similar intensification of the subpolar gyre is observed in the NCEP–NCAR fields when they are subsetted on the periods 1945–79 and 1980–93, respectively. The difference in gyre structure impacts the wind-driven ocean response, January mean Ekman upwelling velocities in the center of the subpolar gyre deduced from SOC and HR are 18.9 and 8.6 m month⁻¹, respectively. In the midlatitude North Pacific a single large-scale subpolar gyre is evident in SOC compared with two smaller gyres in HR.

The Ekman transport in HR has been compared with that for SOC, the greatest differences occur in the Tropical Pacific. At 10°N in this basin the difference in Ekman transports between SOC (32.6 Sv) and HR (41.2 Sv) is large and has a significant impact on the heat transport across the section, amounting to a reduction from 0.7 to 0.4 PW of the estimate of Wijffels et al. (1996). Interannual variability in the Ekman transport has been quantified and at several locations, particularly the midlatitude North Atlantic in winter, the interannual

variability is of the same order as the climatological mean.

We have shown from analysis of the SOC fields that the NAO plays a significant role in driving variability in the wind-driven transport in the North Atlantic. Its impact has been quantified in terms of the difference in vertical Ekman flux between the subpolar and subtropical gyres. As the index becomes more positive, the vertical exchanges in each gyre intensify because the Iceland low drives stronger upwelling and the Azores high stronger downwelling. This amounts to an increase in the vertical volume flux difference between the two gyres of 1.5 Sv per unit increase in the NAO index, with the correlation of the NAO to the subpolar gyre ($r^2 = 0.43$) being slightly stronger than that for the subtropical gyre ($r^2 = 0.38$). Similar results are obtained using the NCEP–NCAR fields and the high level of correlation between them and SOC indicates that the relatively low sampling rate is not a major problem when using the SOC dataset to evaluate the wind-driven forcing of the ocean at gyre scales in the North Atlantic.

Future comparative studies of ship and model wind stress fields and further validations against research buoy measurements will enable progress to be made in understanding and rectifying the deficiencies in each dataset, as will comparisons with satellite retrieved estimates of the stress, which we have not considered here. Such studies may also benefit from the results of ocean state estimation exercises, which have the potential to reveal biases in the chosen model forcing fields (Stammer et al. 2002). To conclude, we note that the SOC climatology represents the recent wind forcing of the ocean, has been derived using an experimentally confirmed drag coefficient and contains stress estimates that have been found to be in good agreement with independent research buoy measurements. We therefore expect it to provide a valuable dataset for use in contemporary hydrographic and modeling studies.

Acknowledgments. The work described in this paper was partially funded by a commissioned research project for the Hadley Centre, U. K. Meteorological Office. The authors would like to thank Harry Bryden and the anonymous referees for helpful comments; Steven Worley at the Data Support Section, NCAR and Scott Woodruff at the NOAA/ERL Climate Diagnostics Center for supplying the COADS 1a and extensions for the period 1994–1997; Bob Weller of WHOI for making available the various research buoy datasets; Glenn White of NCEP for supplying the climatological mean NCEP–NCAR fields and Bernard Barnier of LEGI-IMG, Grenoble, for the ECMWF fields. The HR fields were obtained from the International Research Institute for Climate Prediction/Lamont-Doherty Earth Observatory Climate Data Library (<http://ingrid.ldgo.columbia.edu/>). Note that for the NCEP–NCAR variability analyses described in section 3b and 3c the reanalysis data was also obtained from IRI/LDEO. The SOC wind stress fields

are available at <http://www.soc.soton.ac.uk/JRD/MET/fluxclimatology.html>. The Hurrell NAO index values were obtained from http://goldhill.cgd.ucar.edu/cas/climind/nao_winter.html.

REFERENCES

- Bacon, S., 1997: Circulation and fluxes in the North Atlantic between Greenland and Ireland. *J. Phys. Oceanogr.*, **27**, 1420–1435.
- Bonekamp, H., G. J. Komen, A. Sterl, P. A. E. M. Janssen, P. K. Taylor, and M. J. Yelland, 2002: Statistical comparisons of observed and ECMWF modeled open ocean surface drag. *J. Phys. Oceanogr.*, **32**, 1010–1027.
- Böning, C. W., R. Dösscher, and H.-J. Isemer, 1991: Monthly mean wind stress and Sverdrup transports in the North Atlantic: A comparison of the Hellerman–Rosenstein and Isemer–Hasse climatologies. *J. Phys. Oceanogr.*, **21**, 221–235.
- Bryden, H. L., and L. M. Beal, 2001: Role of the Agulhas Current in Indian Ocean circulation and associated heat and freshwater fluxes. *Deep-Sea Res., I*, **48**, 1821–1845.
- , D. H. Roemmich, and J. A. Church, 1991: Ocean heat transport across 24°N in the Pacific. *Deep-Sea Res.*, **38**, 297–324.
- Bunker, A. F., 1976: Computations of surface energy flux and annual air-sea interaction cycles of the North Atlantic Ocean. *Mon. Wea. Rev.*, **104**, 1122–1140.
- Chelton, D. B., A. M. Mestas-Nuñez, and M. H. Freilich, 1990: Global wind stress and Sverdrup circulation from the Seasat scatterometer. *J. Phys. Oceanogr.*, **20**, 1175–1205.
- Da Silva, A. M., C. C. Young, and S. Levitus, 1994: *Algorithms and Procedures*. Vol. 1, *Atlas of Surface Marine Data*. NOAA Atlas NESDIS 6, 74 pp.
- Dickson, R., J. Lazier, J. Meincke, and P. Rhines, 1996: Long-term coordinated changes in the convective activity of the North Atlantic. *Decadal Climate Variability: Dynamics and Predictability*, D. A. J. Willebrand, Ed., NATO ASI Series, Vol. 44, Springer-Verlag, 211–262.
- Fairall, C. W., E. F. Bradley, D. P. Rogers, J. B. Edson, and G. S. Young, 1996: Bulk parameterization of air-sea fluxes for TOGA COARE. *J. Geophys. Res.*, **101**, 3747–3764.
- Fanning, A. F., R. J. Greatbatch, A. M. da Silva, and S. Levitus, 1994: Model-calculated seasonal transport variations through the Florida Straits: A comparison using different wind stress climatologies. *J. Phys. Oceanogr.*, **24**, 30–45.
- Geernaert, G. L., 1990: Bulk parametrizations for the wind stress and heat fluxes. *Surface Waves and Fluxes*, Vol. 1, G. L. Geernaert and W. J. Plant, Eds., *Current Theory*, Kluwer, 91–172.
- Gershunov, A., and T. Barnett, 1998: Interdecadal modulation of ENSO teleconnections. *Bull. Amer. Meteor. Soc.*, **79**, 2715–2725.
- Gill, A. E., 1982: *Atmosphere–Ocean Dynamics*. Academic Press, 662 pp.
- Gleckler, P. J., and B. C. Weare, 1997: Uncertainties in global ocean surface heat flux climatologies derived from ship observations. *J. Climate*, **10**, 2764–2781.
- Gordon, C., and R. A. Corry, 1991: A model simulation of the seasonal cycle in the tropical Pacific Ocean using climatological and modeled surface forcing. *J. Geophys. Res.*, **96**, 847–864.
- Gulev, S. K., and L. Hasse, 1998: North Atlantic wind waves and wind stress fields from voluntary observing ship data. *J. Phys. Oceanogr.*, **28**, 1107–1130.
- Hall, M. M., and H. L. Bryden, 1982: Direct estimates and mechanisms of ocean heat transport. *Deep-Sea Res.*, **29** (3A), 339–359.
- Harrison, D. E., 1989: On climatological monthly mean wind stress and wind stress curl fields over the World Ocean. *J. Climate*, **2**, 57–70.
- Hellerman, S., and M. Rosenstein, 1983: Normal monthly wind stress over the World Ocean with error estimates. *J. Phys. Oceanogr.*, **13**, 1093–1104.

- Hurrell, J. W., 1995: Decadal trends in the North Atlantic Oscillation—regional temperatures and precipitation. *Science*, **269**, 676–679.
- , and H. van Loon, 1997: Decadal variations in climate associated with the North Atlantic Oscillation. *Climatic Change*, **36**, 301–326.
- Isemer, H.-J., and L. Hasse, 1987: *The Bunker Climate Atlas of the North Atlantic Ocean*. Vol. 2, *Air-Sea Interactions*, Springer-Verlag, 252 pp.
- Josey, S. A., 1999: Seasonal to interannual variability in the SOC air-sea flux dataset and Hadley Centre Atmospheric Model Version 3. Southampton Oceanography Centre Internal Document No. 51, 38 pp. [Available online at <http://www.soc.soton.ac.uk/JRD/MET/PDF/hadam3.pdf>.]
- , 2001: A Comparison of ECMWF, NCEP/NCAR and SOC surface heat fluxes with moored buoy measurements in the subduction region of the north-east Atlantic. *J. Climate*, **14**, 1780–1789.
- , E. C. Kent, and P. K. Taylor, 1998: The Southampton Oceanography Centre (SOC) ocean-atmosphere heat, momentum and freshwater flux atlas. Southampton Oceanography Centre Report 6, 30 pp. [Available online at http://www.soc.soton.ac.uk/JRD/MET/PDF/SOC_flux_atlas.pdf.]
- , —, and —, 1999: New insights into the ocean heat budget closure problem from analysis of the SOC air-sea flux climatology. *J. Climate*, **12**, 2856–2880.
- Kallberg, P., 1997: *Aspects of the Re-analysed Climate*. ECMWF Re-Analysis Project Report Series, Part 2, European Centre for Medium-Range Weather Forecasts, 89 pp.
- Kalnay, E., and Coauthors, 1996: The NCEP/NCAR 40-Year Reanalysis Project. *Bull. Amer. Meteor. Soc.*, **77**, 437–471.
- Kaufeld, L., 1981: The development of a new Beaufort equivalent scale. *Meteor. Rundsch.*, **34**, 17–23.
- Kent, E. C., and P. K. Taylor, 1997: Choice of a Beaufort Equivalent Scale. *J. Atmos. Oceanic Technol.*, **14**, 228–242.
- , —, B. S. Truscott, and J. S. Hopkins, 1993a: The accuracy of voluntary observing ships meteorological observations—results of the VSOP—NA. *J. Atmos. Oceanic Technol.*, **10**, 591–608.
- , R. J. Tiddy, and P. K. Taylor, 1993b: Correction of marine air temperature observations for solar radiation effects. *J. Atmos. Oceanic Technol.*, **10**, 900–906.
- , P. G. Challenor, and P. K. Taylor, 1999: A statistical determination of the random observational errors present in voluntary observing ships meteorological reports. *J. Atmos. Oceanic Technol.*, **16**, 905–914.
- , P. K. Taylor, and P. G. Challenor, 2000: The effect of successive correction on variability estimates for climatological datasets. *J. Climate*, **13**, 1845–1857.
- Klein, B., R. L. Molinari, T. J. Mueller, and G. Siedler, 1995: A transatlantic section at 14.5°N: Meridional volume and heat fluxes. *J. Mar. Res.*, **53**, 929–957.
- Large, W. G., and S. Pond, 1981: Open ocean momentum flux measurements in moderate to strong winds. *J. Phys. Oceanogr.*, **11**, 324–336.
- Leetmaa, A., and A. F. Bunker, 1978: Updated charts of the mean annual wind stress, convergences in the Ekman Layers, and Sverdrup transports in the North Atlantic. *J. Mar. Res.*, **36**, 311–322.
- Lindau, R., 1995: A new Beaufort equivalent scale. *Int. COADS Winds Workshop*, Kiel, Germany, Environmental Research Laboratory, NOAA, 232–252.
- Mantua, N. J., S. R. Hare, Y. Zhang, J. M. Wallace, and R. C. Francis, 1997: A Pacific interdecadal climate oscillation with impacts on salmon production. *Bull. Amer. Meteor. Soc.*, **78**, 1069–1079.
- McPhaden, M. J., and Coauthors, 1998: The Tropical Ocean Global Atmosphere observing system: A decade of progress. *J. Geophys. Res.*, **103**, 14 169–14 240.
- Megann, A. P., and A. L. New, 2001: The effects of resolution and viscosity in an isopycnic-coordinate model of the equatorial Pacific. *J. Phys. Oceanogr.*, **31**, 1993–2018.
- Mestas-Nunez, A. M., D. B. Chelton, M. H. Freilich, and J. G. Rich-
- man, 1994: An evaluation of ECMWF-based climatological wind stress fields. *J. Phys. Oceanogr.*, **24**, 1532–1549.
- Milliff, R. F., W. G. Large, J. Morzel, G. Danabasoglu, and T. M. Chin, 1999: Ocean general circulation model sensitivity to forcing from scatterometer winds. *J. Geophys. Res.*, **104**, 11 337–11 358.
- Moyer, K. A., and R. A. Weller, 1997: Observations of surface forcing from the subduction experiment: A comparison with global model products and climatological data sets. *J. Climate*, **10**, 2725–2742.
- Renfrew, I. A., G. W. K. Moore, P. S. Guest, and K. Bumke, 2002: A comparison of surface layer and surface turbulent flux observations over the Labrador Sea with ECMWF and NCEP reanalyses. *J. Phys. Oceanogr.*, **32**, 383–400.
- Saunders, P. M., 1976: On the uncertainty of wind stress curl calculations. *J. Mar. Res.*, **34**, 155–160.
- Smith, L. T., E. P. Chassignet, and R. Bleck, 2000: The impact of lateral boundary conditions and horizontal resolution on North Atlantic water mass transformations and pathways in an isopycnic coordinate ocean model. *J. Phys. Oceanogr.*, **30**, 137–159.
- Smith, S. D., 1980: Wind stress and heat flux over the ocean in gale force winds. *J. Phys. Oceanogr.*, **10**, 709–726.
- , 1988: Coefficients for sea surface wind stress, heat flux and wind profiles as a function of wind speed and temperature. *J. Geophys. Res.*, **93**, 15 467–15 474.
- , 1989: Water vapour flux at the sea surface. *Bound.-Layer Meteor.*, **47**, 277–293.
- Smith, S. R., D. M. Legler, and K. V. Verzone, 1999: Quantifying uncertainties in NCEP reanalyses using high-quality research vessel observations. *Proc. Second Int. Conf. on Re-Analyses*, Reading, United Kingdom, ECMWF, 133–136.
- Speer, K. G., J. Holfort, T. Reynaud, and G. Siedler, 1996: South Atlantic heat flux at 11°S. *The South Atlantic: Present and Past Circulation*, G. Wefer et al., Eds., Springer Verlag.
- Stammer, D., C. Wunsch, R. Giering, C. Eckert, P. Heimbach, J. Marotzke, A. Adcroft, C. N. Hill, and J. Marshall, 2001: The global ocean circulation during 1992–1997, estimated from ocean observations and a general circulation model. *J. Geophys. Res.*, in press.
- Stricherz, J. N., D. M. Legler, and J. J. O'Brien, 1997: *TOGA Pseudo-Stress Atlas 1985–1994: II Tropical Pacific Ocean*, COAPS/Florida State University, 162 pp.
- Sturges, W., B. G. Hong, and A. J. Clarke, 1998: Decadal forcing of the North Atlantic subtropical gyre. *J. Phys. Oceanogr.*, **28**, 659–668.
- Taylor, P. K., and M. J. Yelland, 2000: A note on the apparent “imbalance” term in the Turbulent Kinetic Energy Budget. *J. Atmos. Oceanic Technol.*, **17**, 82–89.
- , and —, 2001: The dependence of sea surface roughness on the height and steepness of the waves. *J. Phys. Oceanogr.*, **31**, 572–590.
- , E. C. Kent, M. J. Yelland, and B. I. Moat, 1995: The accuracy of wind observations from ships. *Proc. Int. COADS Winds Workshop*, Kiel, Germany, Environmental Research Laboratory, NOAA, 132–155.
- , —, —, and —, 1999: The accuracy of marine surface winds from ships and buoys. *CLIMAR 99, WMO Workshop on Advances in Marine Climatology*, Vancouver, BC, Canada, World Meteorological Organization, 59–68.
- Trenberth, K. E., and J. G. Olson, 1988: An evaluation and intercomparison of global analyses from the National Meteorological Centre and the European Centre for Medium Range Weather Forecasts. *Bull. Amer. Meteor. Soc.*, **69**, 1047–1057.
- , W. G. Large, and J. G. Olson, 1990: The mean annual cycle in global ocean wind stress. *J. Phys. Oceanogr.*, **20**, 1742–1760.
- Weller, R. A., and S. P. Anderson, 1996: Surface meteorology and air-sea fluxes in the western equatorial warm pool during the TOGA coupled ocean-atmosphere response experiment. *J. Climate*, **9**, 1959–1990.

- , D. L. Rudnick, and N. J. Brink, 1995: Meteorological variability and air-sea fluxes at a closely spaced array of surface moorings. *J. Geophys. Res.*, **100** (C3), 4867–4883.
- , M. F. Baumgartner, S. A. Josey, A. S. Fischer, and J. Kindle, 1998: Atmospheric forcing in the Arabian Sea during 1994–1995: Observations and comparisons with climatology and models. *Deep-Sea Res. II*, **45**, 1961–1999.
- WGASF, 2000: Intercomparison and validation of ocean–atmosphere energy flux fields. Final Report of the Joint WCRP–SCOR Working Group on Air–Sea Fluxes (SCOR Working Group 110), WCRP-112, WMO/TD-No. 1036, WMO, Geneva, 312.
- Wijffels, S. E., J. M. Toole, H. L. Bryden, R. A. Fine, W. J. Jenkins, and J. L. Bullister, 1996: The water masses and circulation at 10°N in the Pacific. *Deep-Sea Res., I*, **43**, 501–544.
- WMO, 1993: International list of selected, supplementary and auxiliary ships. WMO Report No. 47, WMO, Geneva, various pagination.
- Woodruff, S. D., R. J. Slutz, R. L. Jenne, and P. M. Steurer, 1987: A comprehensive ocean–atmosphere data set. *Bull. Amer. Meteor. Soc.*, **68**, 1239–1250.
- , S. J. Lubker, K. Wolter, S. J. Worley, and J. D. Elms, 1993: Comprehensive Ocean–Atmosphere Data Set (COADS) release 1a: 1980–92. *Earth Syst. Monitor*, **4**, 4–8.
- Wunsch, C., 1999: The interpretation of short climate records, with comments on the North Atlantic and Southern Oscillations. *Bull. Amer. Meteor. Soc.*, **80**, 245–255.
- , and D. Roemmich, 1985: Is the North Atlantic in Sverdrup balance? *J. Phys. Oceanogr.*, **15**, 1876–1880.
- Yelland, M. J., B. I. Moat, P. K. Taylor, R. W. Pascal, J. Hutchings, and V. C. Cornell, 1998: Wind stress measurements from the open ocean corrected for air flow distortion by the ship. *J. Phys. Oceanogr.*, **28**, 1511–1526.
- Zhang, Y., J. M. Wallace, and D. S. Battisti, 1997: ENSO-like interdecadal variability: 1900–93. *J. Climate*, **10**, 1004–1020.